APERTURE BLOCKING

OF A

SYMMETRIC PARABOLIC REFLECTOR ANTENNAS

BY

MOHAMED SAID A. SANAD

A thesis submitted to the Faculty of Graduate Studies of the University of Manitoba in partial fulfillment of the requirements of the degree of

MASTER OF ENGINEERING

Department of Electrical Engineering
University of Manitoba
July 1982

APERTURE BLOCKING

OF A

SYMMETRIC PARABOLIC REFLECTOR ANTENNAS

BY

MOHAMED SAID A. SANAD

A thesis submitted to the Faculty of Graduate Studies of the University of Manitoba in partial fulfillment of the requirements of the degree of

MASTER OF ENGINEERING

ABSTRACT

The performance of symmetric parabolic reflector antennas is investigated. Mathematical expressions for unblocked and blocked reflector pattern calculations using current distribution method are provided. Struts of circular cross-section are chosen and their blocking equations, based on the induced field ratio hypothesis, are presented. Computed co-polar and cross-polar patterns are then provided for both linearly and circularly polarized $\cos^m \theta$ feed patterns.

Possible methods for reducing the sidelobe levels are discussed. One method that promises to be practical involves the modification of the reflector field phase which illuminate the struts. To accomplish this phase change it is recommended that the reflector be loaded by narrow strips just under each strut. By modifying the thickness of the strips and computing the reflector overall patterns, it is found that for certain strip thicknesses the reflector gain is increased and the pattern sidelobes are reduced to below their level for an unblocked reflector. It is then recommended that this method be verified experimentally.

ACKNOWLEDGEMENTS

I wish to express my sincere appreciation to Dr. L. Shafai of the Electrical Engineering Department, University of Manitoba, for his cheerful guidance, helpful advice, continuous interest and encouragement through all phases of this work.

The financial assistance provided by the Communication Research Centre and the Department of Electrical Engineering of the University of Manitoba are gratefully acknowledged.

TABLE OF CONTENTS

LIST OF SYMBOLS

Unless otherwise stated, the symbols most commonly used in this thesis have the following meaning.

SYMBOL	
IFR	Induced field ratio.
IFR_E	Induced field ratio for wave with the E-vector parallel to the cylinder axis.
E_o	The uniform reference aperture field.
$\eta = 120\pi$	The characteristic impedance of free space.
K	Wave number.
IFR_H	Induced field ratio for the H-vector of the incident plane wave parallel to the cylinder axis.
J_n	Bessel function of order n.
J_n'	Derivative of the Bessel function with respect to its argument.
$H_n^{(2)}$	Hankel function of the second kind of order n.
$H_n^{(2)'}$	Derivative of the Hankel function of the second kind with respect to its argument.
α	Angle between the incident wavefront and the cylinder axis.
GTD	Geometrical theory of diffraction.
x,y,z	Cartesian coordinates of a point S on the reflector.
π,θ',ϕ'	Spherical coordinates of the point S on the reflector.
$\underline{\vec{n}}$	Outward unit normal to the surface of the paraboloid.
F	Focal length of the paraboloid.
$\underline{E}_{inc}^{y-pol}$	E-vector of the incident field when incident wave is linearly polarized along the y-axis.
$\underline{H}_{inc}^{y-pol}$	H-vector of the incident field when incident wave is linearly polarized along the y-axis.

$\underline{E}_{inc}$	E-vector of the incident field.
$\underline{H}_{inc}$	H-vector of the incident field.
$\underline{J}_s$	Surface current density.
$\underline{E}_{ref}$	E-vector of the reflected field.
$\underline{H}_{ref}$	H-vector of the reflected field.
$\underline{E}_{ref}^{y-pol}$	E-vector of the reflected field when reflected wave is linearly polarized along the y-axis.
$\underline{H}_{ref}^{y-pol}$	H-vector of the reflected field when reflected wave is the y-axis.
$\underline{H}_{aper}^{y-pol}$	Aperture field when illuminating wave is linearly polarizd along the y-axis.
$\underline{E}(p)$	The far-zone radiated field at point (p).
R,θ,ϕ	Spherical coordinates of the observation point (p).
$E_\theta^{y-pol}(p)$	θ-component of $\underline{E}(p)$ which is linearly polarized along the y-axis.
$E_\phi^{y-pol}(p)$	ϕ-component of $\underline{E}(p)$ which is linearly polarized along the y-axis.
$\underline{E}_{inc}^{x-pol}$	E-vector of the incident field which is linearly polarized along the x-axis.
$\underline{H}_{inc}^{x-pol}$	H-vector of the incident field which is linearly polarized along the x-axis.
$E_\theta^{x-pol}(p)$	θ-component of the far-zone radiated field, at the point p, which is x-polarized.
$E_\phi^{x-pol}(p)$	ϕ-component of the far-zone radiated field, at the point p, which is x-polarized.
θ_o	θ-angle of any point on the edge of the paraboloid.

ϕ_o	The strut plane.
L	The strut length.
a	The strut radius.
w	The strut diameter.
R_c	The central blockage radius.
$\delta\theta$	The half angle subtended by the central blockage from the reflector centre.
$R^{y\text{-pol}}$	Co-polarized component of the y-polarized field.
$C^{y\text{-pol}}$	Cross-polarized component of the y-polarized field.
$R^{x\text{-pol}}$	Co-polarized component of the x-polarized field.
$C^{x\text{-pol}}$	Cross-polarized component of the x-polarized field.
$\underline{\underline{E}}_{inc}^{circl\text{-}pol}$	Circularly polarized incident field.
$\underline{E}^{circl\text{-}pol}$	Circularly polarized radiated field.
$E_\theta^{circl\text{-}pol}$	θ-component of $\underline{E}^{circl\text{-}pol}$.
$E_\phi^{circl\text{-}pol}$	ϕ-component of $\underline{E}^{circl\text{-}pol}$.
$\lvert c \rvert$	Magnitude of the co-polarized component of the circularly polarized field.
$\lvert d \rvert$	Magnitude of the cross-polarized component of the circularly polarized field.
D	Reflector diameter.
λ	Wavelength.
dB	Decibell.
γ	Thickness of the reflector coating strips.

LIST OF TABLES

LIST OF FIGURES

CHAPTER I

INTRODUCTION

Pencil-beam antennas are widely used in point-to-point microwave communication systems due to their maximum boresight gain. There are several possible techniques for producing pencil beams. The simplest in conception and from the point of view of practical design is that of placing a point source at the focus of an optical system such as a paraboloidal reflector to produce a beam of parallel rays [1]. The parabolic reflector is the only reflector that has the property of giving a collimated beam from a point source located at its focus. Other types of reflectors that can also be used to generate pencil beams are the spherical, stepped, polarized and the lensed reflectors. However, these systems are more complex and are usually used for improving the scanning capability of the system [2].

There are four main reflector configurations, using a single feed, which may be considered for the generation of pencil beams, Fig. 1.1. They comprise the on-axis fed single-reflector and dual reflector antennas, and their offset-fed equivalents. All of these geometries are in use, and each can have specific advantages and disadvantages [3, 4].

On-axis front-fed single reflector, Fig. 1.1(a), is simple to design and inexpensive to fabricate. However, the aperture blockage by the primary feed with its supporting struts leads to scattered radiation

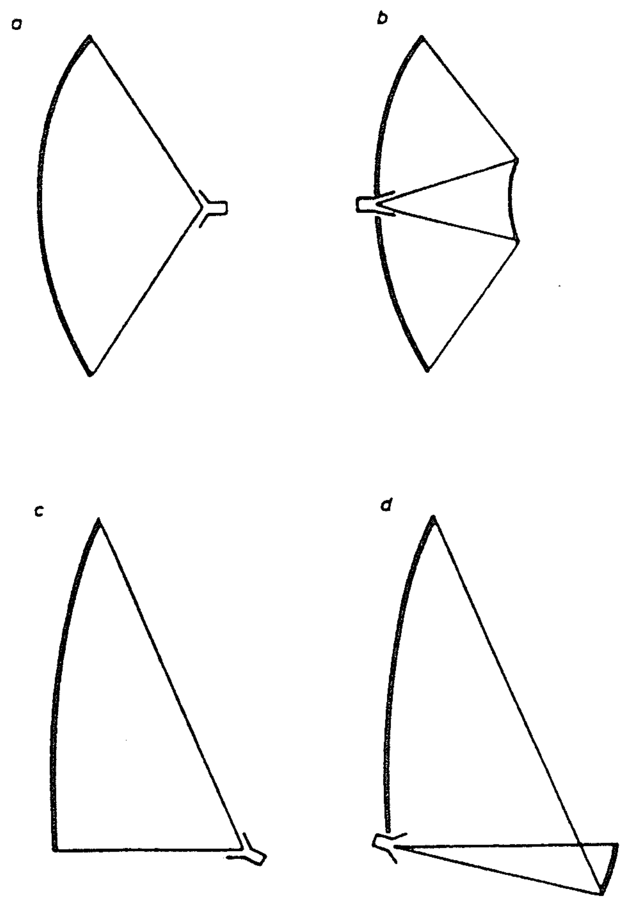

Figure 1.1. Four reflector configurations for pencil - beam applications

(a) on - axis front - fed reflector

(b) on - axis dual reflector

(c) offset front - fed reflector

(d) offset two - reflector antenna

which results in decrease of the antenna gain and increase of the sidelobe and the cross-polarized radiation levels. Also, the front location of the feed makes it difficult to be reached for servicing purposes.

The dual-reflector systems are also commonly used with the Cassegrainian antanna, Fig. 1.1(b), being the most common one. The main disadvantage of the Cassegrainian antenna is the spillover from the real feed past the edge of the subdish and its supporting structure.

An alternative solution to the supporting structure problem is the use of offset systems, Fig. 1.1(c) and Fig. 1.1(d). Structurally, the asymmetry of the offset reflector is considered as a major drawback because it is more difficult to deal with and, in any case, is more costly to implement. Also, when illuminated by a conventional linearly polarized primary feed the offset reflector will generate a cross-polarized component in the radiation field and when circular polarization is employed, the antenna beam is squinted from the electrical boresight. For small offset reflectors this squinting effect has also been observed with linear polarization [4].

Generally, the choice of optimum reflector configuration depends on the kind of application in which it will be used and design requirements of that application. For small earth-station antennas, the symmetric front-fed paraboloid is a distinctly economic choice because of the ease of fabrication of the reflector and the low cross-polarization of the radiated field [5].

As mentioned before, the main disadvantage of the symmetric parabolic reflector antenna is the aperture blocking. The presence of an object in front of a reflector antenna will cause significant changes in its radiation characteristics. These objects may be classified as (a) large, centrally located objects such as a feed horn, and (b) long, thin cylinderical structures (struts) used for mechanical support of the central object, Fig. 1.2.

Early analysis of the effects of strut blocking have been based on the null-field hypothesis [6], i.e. that the currents on the shadowed portions of the surface are non-radiative. Rather elaborate geometrical constructions have been made to determine the shape of various shadows caused by quasi-planar or quasi-spherical wavefronts in the immediate vicinity of the reflector [7]. However, this approach fails to take into account the depth, cross-section, or tilt of the struts, nor does it provide any differences for frequency or polarization effects. Furthermore, the struts generally have widths of the order of a wavelength, so that no basis exists for the expectation that deep, clearly defined optical shadows will be cast by the various waves impinging on the struts.

The induced field ratio (IFR) hypothesis used by Rusch and Sorensen [8, 9], does not employ the concept of the shadows, and takes into account cross-section, tilt, polarization, and the frequency. The IFR of an infinitely long cylinderical scatterer is a measure of its forward scattered field when it is immersed in an incident plane wave. When an infinite cylinder is immersed in an incident plane wave, Fig. 1.3, the IFR is defined

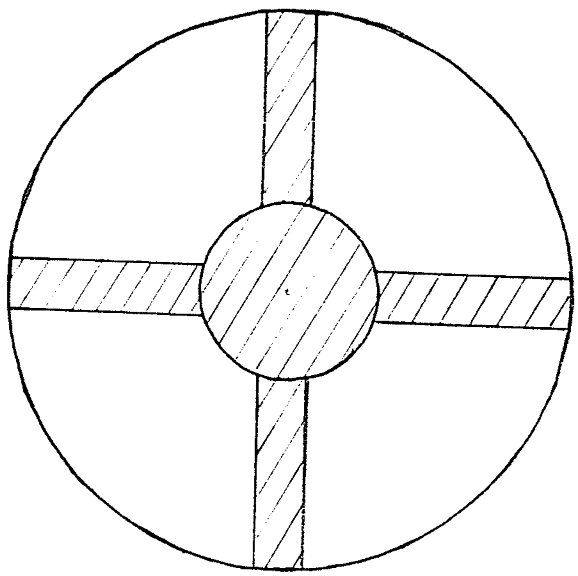

Figure 1.2. Geometry of aperture blockage of reflector antenna .

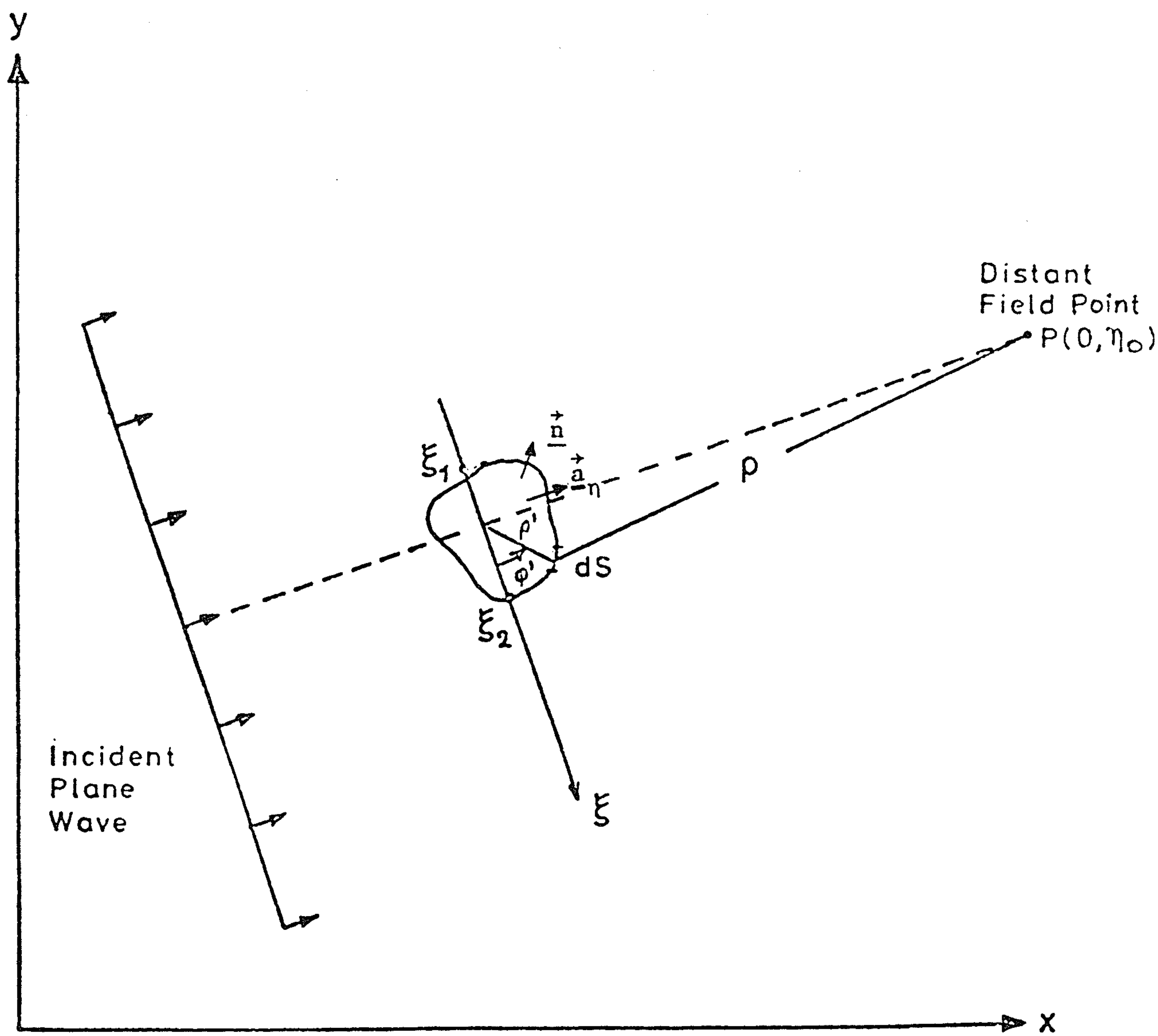

Figure 1.3. Geometry to define Induced - Field - Ratio [Rusch , Hansen , Klein and Mittra , 1976] .

as the ratio of the forward-scattered field to the hypothetical field radiated in the forward direction by the plane wave in the reference aperture of width equal to the shadow of the geometrical cross-section of the cylinder on the incident wavefront. Thus for the E-vector of the incident plane wave parallel to the cylinder axis [8], the IFR can be defined as:

$$\mathrm{IFR}_E = -\frac{\eta}{2(\zeta_2 - \zeta_1)E_o} \int_{S_1} J_{sz}\, e^{jk\rho'} \cos(\phi' - \tfrac{\pi}{2})\, dl \quad \text{..........} (1.1)$$

where E_o is the uniform reference aperture field and $\eta = 120\pi$.

For the H-vector parallel to the cylinder axis it is of the form

$$\mathrm{IFR}_H = \frac{1}{2(\zeta_2 - \zeta_1)H_o} \int_{S_1} H_z\, (\vec{\underline{a}}_\eta \cdot \vec{\underline{n}}) e^{jk\rho'} \cos\left(\phi' - \tfrac{\pi}{2}\right) dl \quad \text{.....}(1.2)$$

The IFR_E and IFR_H for a circular-cylinder of the radius a are given by [2]:

$$\mathrm{IFR}_E = -\frac{1}{Ka\cos\alpha} \sum_{n=-\infty}^{\infty} J_n(Ka\cos\alpha)/H_n^{(2)}(Ka\cos\alpha) \quad \text{......}(1.3)$$

$$\mathrm{IFR}_H = -\frac{1}{Ka\cos\alpha} \sum_{n=-\infty}^{\infty} J_n'(Ka\cos\alpha)/H_n^{(2)\prime}(Ka\cos\alpha) \quad \text{....}(1.4)$$

where J_n is the Bessel function of order n,

$H_n^{(2)}$ is the Hankel function of the second kind of order n,

J_n', $H_n^{(2)\prime}$ are their derivatives with respect to their arguments.

and α is the angle between the incident wavefront and the cylinder axis.

The IRF's for the circular cylinder were plotted by Rusch[9] in the complex plane and are shown in Fig. 1.4. In general, the IFR_E is larger in magnitude than the IFR_H, and has a positive phase angle compared to a

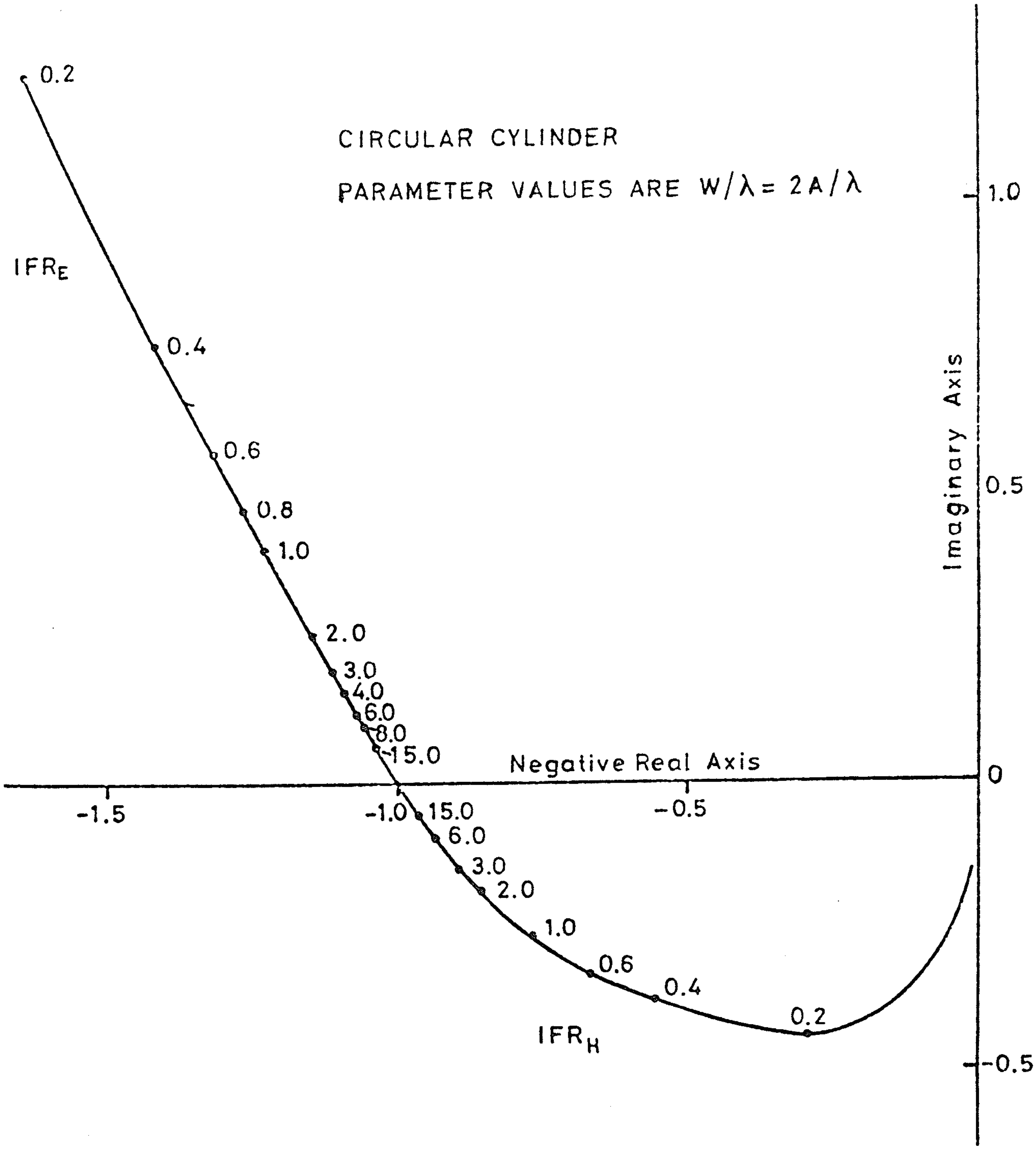

Figure 1.4. Complex IFR_E and IFR_H for a circular cylinder [Rusch , Hansen , Klein and Mittra , 1976] .

nagative phase angle for the H-polarization. Both IRF's approach the value $-1.0 + j\ 0.0$ as the radius increases, one from below and the other from above.

The IFR hypothesis proposes that the strut currents due to the plane wave component of the focal-region field are the same currents that would flow on an infinite cylindrical structure of the same cross-section in free space immersed in an infinite plane wave with the same polarization and direction of incidence as the local geometrical ray incident upon that part of the strut as it emerges from the aperture [10, 11].

The IFR hyothesis seems to be physically reasonable, particularly when the struts are long and thin relative to the wavelength. However, more quantitative confirmation is also available. Kuehl [12] demonstrated that the radiation pattern of a dipole near a finite cylinder can be computed by integrating the currents from the corresponding infinite cylinder over the finite cylinder. Rusch [8], in a two-dimensional analog of the aperture blocking problem, used the method of moments and the IFR hypothesis to determine the currents on two cylinders blocking the aperture of a parabolic reflector with a line-source feed and confirmed the IFR hypothesis.

The central blockage has been usually studied using the surface current cancellation method. The surface current cancellation method is based on simple geometrical concepts which in principle are insufficient to describe antenna characteristics at microwave frequencies. At radio frequencies the shadow produced by an obstacle cannot be accurately described by means of optical concepts. To account for the fact that this shadow is wider, equivalent electric and magnetic line sources have been imposed on the edge of the obstacle [8, 13]. However, when the blocking obstacles are large compared to a wavelength, their effects can usually be described with reasonable accuracy using the geometrical blocking approximation, provided that the angles of observation are not far from boresight [1, 7, 9]. This approximation assumes that the projection of the blocking obstacle onto the reflecting surface cancels contributions to the radiated field from currents on these blocked portions on the surface. Thus the radiation pattern associated with the blocked aperture is the superposition of the pattern of the unblocked aperture and the pattern of the blocked portion of the aperture excited 180° out of phase.

The main purpose of this thesis is to present useful analysis which suitably describes the effect of the aperture blockage and the possible remedies for its effect. In chapter two, the mathematical expressions necessary for the overall reflector pattern calculations are developed for both linearly polarized and circularly polarized feeds. The computed results for some selected cases are presented in chapter three. The possible techniques for the sidelobe reduction are discussed in chapter four. One of these techniques which seems applicable, the aperture field phase shifting method, is applied and a few selected computed results are presented.

CHAPTER II

FORMULATION OF UNBLOCKED AND BLOCKED REFLECTOR FIELD

2.1 INTRODUCTION

Exact solutions of the scattering problem have been obtained for only a limited number of cases involving simple primary fields and reflectors of simple geometry, such as spheres and cylinders. In treating reflectors of arbitrary shape it is necessary to resort to approximate techniques. The most common of such techniques are the current distribution method, the aperture field method and the methods based on the geometrical theory of diffraction.

In the current distribution method, the current distribution over the reflector is obtained on the basis of the geometrical optics, which yields good results only if the reflector surface is smooth and its diameter is generally large with respect to the wavelength. This method assumes that there is no current over the shadow area of the reflector. The current distribution over the illuminated region is obtained on the assumption that at every point the incident field is reflected as though an infinite plane wave were incident on the infinite tangent plane. Once the current distribution is obtained all the important characteristic properties may be determined easily [1]. The current distribution method has the advantage of leading to a good approximation for the scattered field. The aperture field method determines the distribution of the tangential electric field on the focal plane projected aperture. This method has no special advantages over the current distribution method. It just leads to simpler mathematical expressions [1].

The geometrical theory of diffraction (GTD) treats diffraction as a localized phenomena, and allows one to obtain the scattered field directly from purely geometrical considerations. Using simple ray tracing, one can include cotributions to the scattered field due to geometrical optics reflection as well as diffraction fields from edges and corners [14]. Tsai [15] in comparing between the integral equation methods and the GTD showed that integral equation methods are more accurate for small structures, are applicable to a wide range of geometric configurations, and provide more information (current, impedance, ... etc).

Generally, for computation of the reflector field near the main axis, the current distribution method provides a convenient approach. Since in this work we are mainly concerned with the near-in-sidelobes and the reflector boresight gain, this method will be used throughout this thesis.

2.2 Unblocked Reflector Field With A Linearly Polarized Feed

The geometry of a paraboloidal reflector is shown in Fig. 2.1. The origin of coordinates is the paraboloid focus. The z-axis is the axis of symmetry. If x, y, z are the cartesian coordinates of a point S on the reflector and ρ, θ', ϕ' are the spherical coordinates of the same point, F is the focal length, and $\underline{\vec{n}}$ is the outward unit normal to the surface of the paraboloid, then:

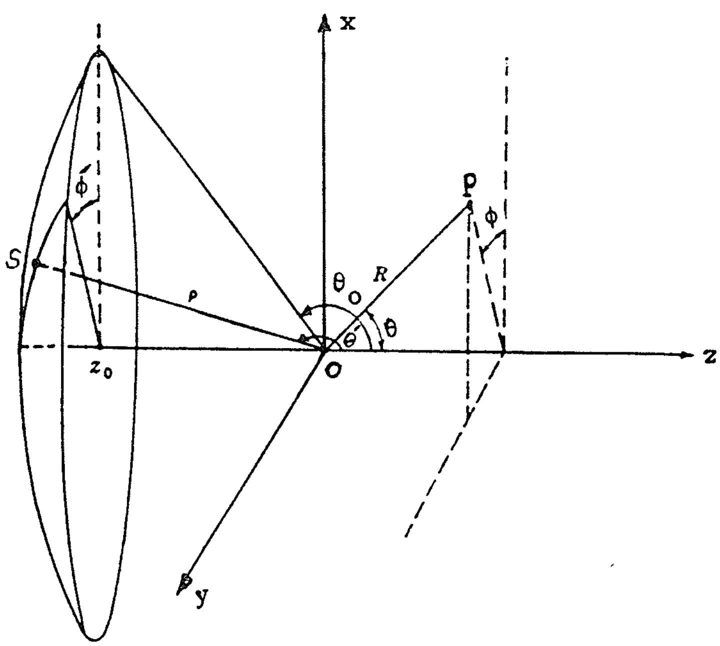

Figure 2.1. Paraboloid geometry .

$$\left.\begin{aligned}\rho &= 2F + z = F + \frac{x^2 + y^2}{4F} \\ &= \frac{2F}{1 - \cos\theta'}\end{aligned}\right\} \qquad (2.1)$$

$$\left.\begin{aligned}\vec{\underline{n}} &= -\cos\phi' \cos\frac{\theta'}{2}\, \vec{\underline{e}}_x - \sin\phi' \cos\frac{\theta'}{2}\, \vec{\underline{e}}_y + \sin\frac{\theta'}{2}\, \vec{\underline{e}}_z \\ &= -\sin\frac{\theta'}{2}\, \vec{\underline{e}}_\rho - \cos\frac{\theta'}{2}\, \vec{\underline{e}}_{\theta'}\end{aligned}\right\} \qquad (2.2)$$

$$\left.\begin{aligned}ds &= dxdy/\sin\frac{\theta'}{2} \\ &= \rho^2 \sin\theta'\, d\theta'\, d\phi'/\sin\frac{\theta'}{2}\end{aligned}\right\} \qquad (2.3)$$

Consider that the incident field is the far zone field of a circular aperture excited in the m = 1 mode. If the incident field is linearly polarized along the y-axis then it can be written as:

$$\underline{E}_{inc}^{y\text{-}pol} = \frac{e^{-jk\rho}}{\rho} \left[a_1(\theta') \sin\phi' \vec{\underline{e}}_{\theta'} + d_1(\theta') \cos\phi'\, \vec{\underline{e}}_{\phi'}\right] \qquad (2.4)$$

$$\underline{H}_{inc}^{y\text{-}pol} = \frac{e^{-jk\rho}}{\eta\rho} \left[- d_1(\theta') \cos\phi'\, \vec{\underline{e}}_{\theta'} + a_1(\theta') \sin\phi'\, \vec{\underline{e}}_{\phi'}\right] \qquad (2.5)$$

The polar patterns $a_1(\theta')$ and $d_1(\theta')$ are assumed to be such that most of the energy is radiated toward the reflector and very little energy is radiated in the half-space z>0. Furthermore to assure continuity of the field when $\theta' = \pi$ it is necessary that

$$d_1(\pi) = - a_1(\pi) \qquad (2.6)$$

According to the laws of the geometrical optics the current density $\underline{J}_S$ is given by

$$\underline{J}_s = \begin{cases} 0 & \text{on the back of the reflector} \\ 2(\vec{\underline{n}} \times \underline{H}_{inc}) & \text{on the front of the reflector} \end{cases} \quad \text{..............(2.7)}$$

An application of equation (2.4) shows the geometrical optics current density on the front of the reflector to be [1]:

$$\underline{J}_s^{y\text{-pol}} = \frac{2}{\eta} \cdot \frac{e^{-jk\rho}}{\rho} \{C_x \vec{\underline{e}}_x + C_y \vec{\underline{e}}_y + C_z \vec{\underline{e}}_z\} \quad \text{..................(2.8)}$$

where

$$C_x = - \sin \frac{\theta'}{2} \sin \phi' \cos \phi' [a_1(\theta') + d_1(\theta')] \text{..................(2.9)}$$

$$C_y = - \sin \frac{\theta'}{2} [a_1(\theta') \sin^2 \phi' - d_1(\theta') \cos^2 \phi'] \text{................(2.10)}$$

$$C_z = - \cos \frac{\theta'}{2} \sin \phi' \, a_1(\theta') \text{..................................(2.11)}$$

By making the feed pattern axially symmetric, i.e.

$$d_1(\theta') = - a_1(\theta') \text{ for } \theta'_o \leq \theta' \leq \pi, \text{ ....(2.12)}$$

where θ'_o is the angle of the points on the circular edge of the paraboloid, we then have

$$\underline{J}_s^{y\text{-pol}} = \frac{2e^{-jk\rho}}{\eta\rho} \{- \sin \frac{\theta'}{2} \vec{\underline{e}}_y - \cos \frac{\theta'}{2} \sin \phi' \vec{\underline{e}}_z\} \, a_1(\theta') \text{..(2.13)}$$

Similarly, the ray-optical reflected field may be computed from

$$\underline{E}_{ref} = - \underline{E}_{inc} + 2(\vec{\underline{n}} \cdot \underline{E}_{inc}) \vec{\underline{n}} \text{ ....(2.14)}$$

yielding

$$\underline{E}_{ref}^{y\text{-pol}} = \{\frac{e^{-jk\rho}}{\rho}\}\{\vec{\underline{e}}_x \sin \phi' \cos \phi' (a_1 + d_1) + \vec{\underline{e}}_y (a_1 \sin^2 \phi' - d_1 \cos^2 \phi')\} \text{.(2.15)}$$

This field propagates rectilinearly parallel to the z-axis producing the focal plane field:

$$\underline{E}_{aper}^{y\text{-pol}} = \frac{e^{-jK2F}}{\rho} \{\vec{e}_x \sin \phi' \cos \phi' (a_1 + d_1) + \vec{\underline{e}}_y (a_1 \sin^2 \phi' - d_1 \cos^2 \phi')\} \text{.(2.16)}$$

The far-zone fields radiated by the currents induced on the scatterer are from equation

$$\underline{E}(p) = -\frac{jw\mu}{4\pi}\frac{e^{-jkR}}{R}\int\left[\underline{J}_s - (\underline{J}_s \cdot \vec{\underline{e}}_r)\vec{\underline{e}}_r\right] e^{jk\rho\vec{\underline{e}}_\rho \cdot \vec{\underline{e}}_r}\, ds \quad \text{................(2.17)}$$

If $\underline{J}_s$ is approximated by the geometrical current density in equation (2.13) then the resulting physical-optics approximation of the field is

$$E_\theta^{y\text{-pol}}(P) = jkF \sin\phi \frac{e^{-jkR}}{R}\int_{\pi-\theta_o}^{\pi}\frac{e^{-jk\rho(1-\cos\theta\cos\theta')}}{(1-\cos\theta')}\Big\{a_1\cos\theta\,[J_o(\beta)-J_2(\beta)] - d_1\cos\theta[J_o(\beta)+J_2(\beta)] - 2j\sin\theta\cot\frac{\theta'}{2}\,J_1(\beta)\,a_1\Big\}\sin\theta'\,d\theta' \quad \text{...(2.18)}$$

$$E_\phi^{y\text{-Pol}}(P) = jKF\cos\phi\frac{e^{-jKR}}{R}\int_{\pi-\theta_o}^{\pi}\frac{e^{-jK\rho(1-\cos\theta\cos\theta')}}{(1-\cos\theta')}\Big\{a_1[J_o(\beta)+J_2(\beta)] - d_1[J_0(\beta)-J_2(\beta)]\Big\}\sin\theta'\,d\theta' \quad \text{..................(2.19)}$$

where J is the Bessel function and $\beta = K\rho\sin\theta\sin\theta'$.

Now if the incident field is linearly polarized along x-axis, then it can be written as:

$$\underline{E}_{inc}^{x\text{-pol}} = \frac{e^{-jk\rho}}{\rho}\left[-d_1(\theta')\cos\phi'\,\vec{\underline{e}}_\theta + a_1(\theta')\sin\phi'\,\vec{\underline{e}}_\phi\right] \quad \text{.............(2.20)}$$

$$\underline{H}_{inc}^{x\text{-pol}} = \frac{e^{-jk\rho}}{\rho}\left[-a_1(\theta')\sin\phi'\,\vec{\underline{e}}_\theta - d_1(\theta')\cos\phi'\,\vec{\underline{e}}_\phi\right] \quad \text{..............(2.21)}$$

Following the same procedure we get the physical-optics approximation of the field as:

$$E_\theta^{x\text{-pol}}(P) = -jKF\cos\phi\frac{e^{-jKR}}{R}\int_{\pi-\theta_o}^{\pi}\frac{e^{-jK\rho(1-\cos\theta\cos\theta')}}{(1-\cos\theta')}\cdot\Big\{d_1\cos\theta\,\cdot$$

$$[J_o(\beta) - J_2(\beta)] - a_1 \cos\theta [J_o(\beta) + J_2(\beta)] - 2j \sin\theta$$

$$\cot\frac{\theta'}{2} \; J_1(\beta) d_1 \} \sin\theta' d\theta' \quad \text{.......................(2.22)}$$

$$E_\phi^{x-pol}(P) = jKF \sin\phi \frac{e^{-jK\rho}}{\rho} \int_{\pi-\theta_o}^{\pi} \frac{e^{-jK\rho(1 - \cos\theta \cos\theta')}}{(1 - \cos\theta')} \{d_1[J_o(\beta) + J_2(\beta)]$$

$$- d_1 [J_o(\beta) - J_2(\beta)]\} \sin\theta' \, d\theta' \quad \text{...........................(2.23)}$$

2.3 Strut Field with a Linearly Polarized Feed

The geometry of a single, perfectly conducting strut is shown in Fig. 2.2, where the strut axis lies in the plane $\phi' = \phi_o$. The strut lies at an angle α $(-90° < \alpha < 90°)$ with respect to the r' - axis, which is perpendicular to z' in the plane $\phi' = \phi_o$. The (cylinderical) strut lies entirely on one side of the z-axis with, at most, one end touching the z-axis. The end of the strut axis lying closer to the z'-axis has coordinates (r_1', z_1'), and the other end has coordinates (r_2', z_2'), where $r_1' \geq o$, $r_2' \geq o$, $r_1' < r_2'$. Thus

$$\alpha = \tan^{-1} \left[\frac{z_2' - z_1'}{r_2' - r_1'}\right] \quad \text{.......................................(2.24)}$$

and the strut length is

$$L = \left[(r_2' - r_1')^2 + (z_2' - z_1')^2\right]^{1/2} \quad \text{............................(2.25)}$$

The incident plane wave is emerging from the reflector with $\underline{K}=K\vec{\underline{e}}_{z'}$, i.e. in the positive z' direction. The right handed x"-y"-z" coordinate system is also shown in the Fig. 2.2. The angle ϕ" measured about the z"-axis, in the x"-y" plane, from the x"-axis.

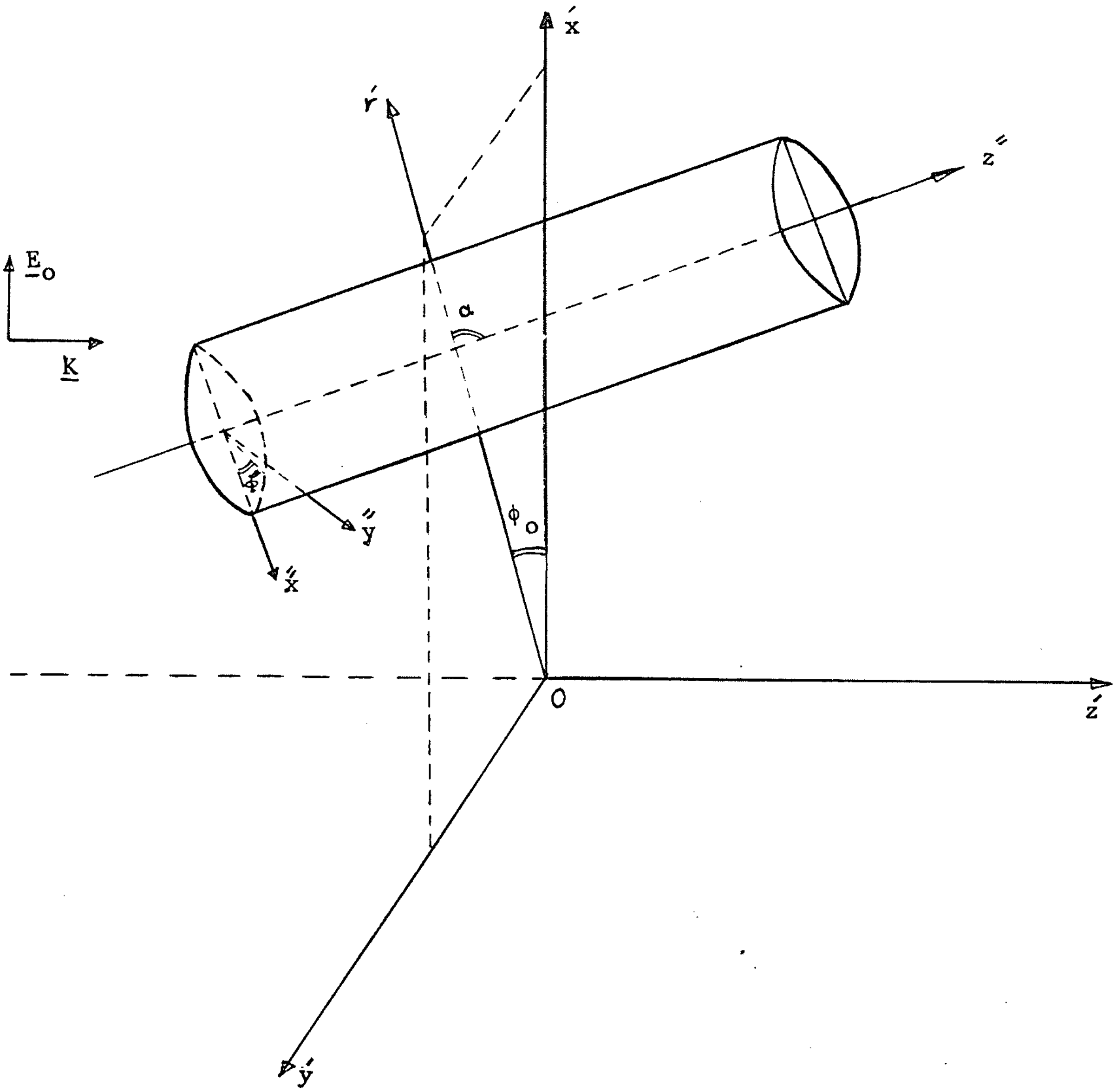

Figure 2.2. Strut geometry .

2.3.1 E-Polarization

We will assume that the strut have a circular cross section of radius a. It will be also assumed that the E-vector of the incident plane-wave lies in the plane $\phi' = \phi_0$. Under these conditions Rusch and Sorensen [8] showed that the scattered field due to the strut current is given by

$$\underline{E}(P) = \left(\frac{jK}{2\pi}\right)\left(\frac{e^{-jKR}}{R}\right) e^{jP_o} \left\{\underline{e}_o \, \mathrm{IFRE}(D,\delta,\alpha)\right\}$$

$$2a \int_{r_1'}^{r_2'} E_A(r') e^{jKr'A_o} \, dr' \ldots\ldots\ldots\ldots\ldots\ldots\ldots (2.26)$$

where

$$\underline{e}_o = \left[\cos\theta \cos(\phi - \phi_o) - \tan\alpha \sin\theta\right] \vec{\underline{e}}_\Theta - \sin(\phi - \phi_o)\vec{\underline{e}}_\phi \ldots\ldots (2.27)$$

$$P_o = (Kz'_1 - Kr'_1 \tan\alpha)(\cos\theta - 1) \ldots\ldots\ldots\ldots\ldots\ldots\ldots (2.28)$$

$$A_o = \sin\theta \cos(\phi - \phi_o) + \tan\alpha(\cos\theta - 1) \ldots\ldots\ldots\ldots\ldots (2.29)$$

$$B = \sin\alpha \sin\theta \cos(\phi - \phi_o) - \cos\alpha \cos\theta \ldots\ldots\ldots\ldots\ldots (2.30)$$

$$C = \sin\theta \sin(\phi - \phi_o) \ldots\ldots\ldots\ldots\ldots\ldots\ldots\ldots\ldots\ldots (2.31)$$

$$D = \sqrt{B^2 + C^2} \ldots\ldots\ldots\ldots\ldots\ldots\ldots\ldots\ldots\ldots\ldots\ldots (2.32)$$

$$\delta = \tan^{-1}\left[\frac{-C}{-B}\right] \ldots\ldots\ldots\ldots\ldots\ldots\ldots\ldots\ldots\ldots\ldots (2.33)$$

and $E_A(r')$ is the focal-plane E-field in the r'-direction and the generalized IFR is

$$\mathrm{IFRE}(D, \delta, \alpha) = -\frac{1}{ka\cos\alpha} \sum_{n=-\infty}^{\infty} e^{jn\delta} \frac{J_n(KaD)}{H_n^{(2)}(Ka\cos\alpha)} \ldots\ldots (2.34)$$

2.3.2 H-Polarization

Here we will assume that the component of the H-vector is lying along the strut. In this case, Rusch and Sorensen [8] have shown that the strut field is given by:

$$\underline{E}(P) = \left(\frac{jK}{2\pi}\right)\left(\frac{e^{-jKR}}{R}\right) e^{jP_o} \Big\{\underline{a}_c \ \mathrm{IFRH}(D,\delta,\alpha) + \Big[\frac{\underline{a}_s}{KaD} -$$

$$(\vec{\underline{e}}_\theta a_\theta + \vec{\underline{e}}_\phi a_\phi) \frac{\sin\alpha}{Ka\cos^2\alpha}\Big] \ \mathrm{JFRH}\ (D,\delta,\alpha)\Big\} \cdot$$

$$2a \int_{r_1'}^{r_2'} \eta \ H_A(r') \ e^{jKr'A_o} \ dr' \ldots\ldots\ldots\ldots\ldots(2.35)$$

where

$$\underline{a}_c = \vec{\underline{e}}_\theta \left[\sin\delta\cos\alpha\sin\theta + \sin\delta\sin\alpha\cos\theta\cos(\phi - \phi_o)\right.$$

$$\left. - \cos\delta\cos\theta\sin(\phi - \phi_o)\right] + \vec{\underline{e}}_\phi \left[-\sin\delta\sin\alpha\sin(\phi - \phi_o)\right.$$

$$\left. - \cos\delta\cos(\phi - \phi_o)\right] \ldots\ldots\ldots\ldots\ldots\ldots\ldots\ldots\ldots(2.36)$$

$$\underline{a}_s = \vec{\underline{e}}_\theta \left[\cos\delta\cos\alpha\sin\theta + \cos\delta\sin\alpha\cos\theta\cos(\phi - \phi_o) +\right.$$

$$\left. \sin\delta\cos\theta\sin(\phi - \phi_o)\right] + \vec{\underline{e}}_\phi \left[-\cos\delta\sin\alpha\sin(\phi - \phi_o)\right.$$

$$\left. + \sin\delta\cos(\phi - \phi_o)\right] \ldots\ldots\ldots\ldots\ldots\ldots\ldots\ldots\ldots(2.37)$$

$$a_\theta = \cos\alpha\cos\theta\cos(\phi - \phi_o) - \sin\alpha\sin\theta \ldots\ldots\ldots\ldots\ldots(2.38)$$

$$a_\phi = -\cos\alpha\sin(\phi - \phi_o) \ldots\ldots\ldots\ldots\ldots\ldots\ldots\ldots\ldots(2.39)$$

$$\mathrm{IFRH}(D,\delta,\alpha) = -\frac{1}{Ka\cos\alpha} \sum_{n=-\infty}^{\infty} e^{jn\delta} \frac{J_n'(KaD)}{H_n^{(2)'}(Ka\cos\alpha)} \ldots\ldots\ldots(2.40)$$

$$\mathrm{JFRH}(D,\delta,\alpha) = -\frac{1}{Ka\cos\alpha} \sum_{n=-\infty}^{\infty} jne^{jn\delta} \frac{J_n(KaD)}{H_n^{(2)'}(Ka\cos\alpha)} \ldots(2.41)$$

and $H_A(r')$ is the focal-plane H-field in the r'-direction.

2.4 Central Blockage Field

As mentioned before, in Chapter I, the central blockage has been studied using the surface current cancellation method which gives a reasonable accuracy when the blocking obstacles are large compared to the wavelength and provided that the angles of observation are not far from boresight, which is our case. Thus, the effect of the central blockage can easily be accounted for by modifying the integration range in the formulation of the main reflector fields. That is, in equations (2.18), (2.19), (2.22) and (2.23) one only needs to carry out the numerical integration from $(\pi - \theta_o)$ to $(\pi - \delta\theta)$ where $\delta\theta$ is the half angle subtended by the central blockage from the reflector centre. Assuming the central blockage radius as R_c, this angle is given by:

$$\delta\theta = \tan^{-1} (R_c/F) \qquad (2.42)$$

2.5 Total Reflector Field and its Co-Polar and Cross-Polar Components

An addition of the strut fields, in equations (2.26) and (2.35) to the reflector fields, in (2.18) and (2.19) for the y-polarization or (2.22) and (2.23) for the x-polarization, after modifying the integration range, as mentioned in the last section, gives the total radiated field of a symmetric paraboloid. For an arbitrary polarization of the aperture field, with respect to the struts, a combination of (2.26) and (2.35) must be used, with a proper vectorial addition. Similarly, for multiple strut support the overall strut field must be considered.

Using the third definition of Ludwig [17] for the co-polar, $R^{y\text{-pol}}(\theta,\phi)$, and cross-polar, $C^{y\text{-pol}}(\theta,\phi)$, components of a transmitted field and $\underline{E}^{y\text{-pol}}(\theta,\phi)$ linearly polarized along the y-axis, we get:

$$R^{y\text{-pol}}(\theta,\phi) = \underline{E}^{y\text{-pol}}(\theta,\phi) \cdot \left\{\sin\phi\, \underline{\vec{e}}_\theta + \cos\phi\, \underline{\vec{e}}_\phi\right\} \quad (2.43)$$

$$C^{y\text{-pol}}(\theta,\phi) = \underline{E}^{y\text{-pol}}(\theta,\phi) \cdot \left\{\cos\phi\, \underline{\vec{e}}_\theta - \sin\phi\, \underline{\vec{e}}_\phi\right\} \quad (2.44)$$

If:

$$\underline{E}^{y\text{-pol}}(\theta,\phi) = E_\theta^{y\text{-pol}}(\theta,\phi)\, \underline{\vec{e}}_\theta + E_\phi^{y\text{-pol}}(\theta,\phi)\, \underline{\vec{e}}_\phi \quad (2.45)$$

then:

$$R^{y\text{-pol}}(\theta,\phi) = E_\theta^{y\text{-pol}}(\theta,\phi)\sin\phi + E_\phi^{y\text{-pol}}(\theta,\phi)\cos\phi \quad (2.46)$$

$$C^{y\text{-pol}}(\theta,\phi) = E_\theta^{y\text{-pol}}(\theta,\phi)\cos\phi - E_\phi^{y\text{-pol}}(\theta,\phi)\sin\phi \quad (2.47)$$

If the transmitted field is linearly polarized along the x-axis, then:

$$R^{x\text{-pol}}(\theta,\phi) = -E_\theta^{x\text{-pol}}(\theta,\phi)\cos\phi + E_\phi^{x\text{-pol}}(\theta,\phi)\sin\phi$$

$$C^{x\text{-pol}}(\theta,\phi) = E_\theta^{x\text{-pol}}(\theta,\phi)\sin\phi + E_\phi^{x\text{-pol}}(\theta,\phi)\cos\phi \quad (2.48)$$

2.6 Reflector Field with a Circularly Polarized Feed

If the polarization of the incident wave is circular, then we may express this as the sum of two linearly polarized waves in time quadrature [18]. Thus the field incident on the reflector can be expressed symbolically as:

$$\underline{E}_{inc}^{circl-pol} = E_{inc}^{x-pol}\ \vec{\underline{e}}_x + e^{j\pi/2}\ E_{inc}^{y-pol}\ \vec{\underline{e}}_y \qquad (2.49)$$

In the spherical coordinates, (2.49) can be written as:

$$\underline{E}_{inc}^{circl-pol} = \left(E_{\theta-inc}^{x-pol} + e^{j\frac{\pi}{2}} E_{\theta-inc}^{y-pol} \right) \vec{\underline{e}}_\theta + \left(E_{\phi-inc}^{x-pol} + e^{j\frac{\pi}{2}} E_{\phi-inc}^{y-pol} \right) \vec{\underline{e}}_\phi \qquad (2.50)$$

The θ and ϕ components of the radiated field can now be written as:

$$E_\theta^{circl-pol} = E_\theta^{x-pol} + e^{j\frac{\pi}{2}} E_\theta^{y-pol} = |E_\theta^{circl-pol}| \exp(j\Phi_1) \qquad (2.51)$$

$$E_\phi^{circl-pol} = E_\phi^{x-pol} + e^{j\frac{\pi}{2}} E_\phi^{y-pol} = |E_\phi^{circl-pol}| \exp\ (j\Phi_2) \qquad (2.52)$$

From (2.51) and (2.52) it is seen that the radiated field is elliptically polarized, indicating that the cross-polarization has taken place as expected. The cross-polar component in this case consists of a circularly polarized wave but with its sense of rotation opposite to that of the incident wave. In order to determine the relative magnitude of the cross-polarized field we need to express the radiated field as a sum of two circularly polarized waves: one right hand circular and the other left hand circular. Now, rewriting the expression for the radiated field,

$$\underline{E}^{circl-pol} = |E_\theta^{circl-pol}|\exp(j\Phi_1)\vec{\underline{e}}_\theta + |E_\phi^{circl-pol}|\exp(j\Phi_2)\vec{\underline{e}}_\phi$$

$$= |E_\theta^{circl-pol}|\exp(j\Phi_1)\ [\vec{\underline{e}}_\theta + m\ \exp(j\phi')\vec{\underline{e}}_\phi] \qquad (2.53)$$

where

$$m = |E_\phi^{circl-pol}/E_\theta^{circl-pol}| \qquad (2.54)$$

and

$$\Phi' = \Phi_2 - \Phi_1 \qquad (2.55)$$

Expressing $\underline{E}^{circl-pol}$ as the sum of two circularly polarized waves, we have

$$\underline{E}^{circl-pol} = c[\vec{\underline{e}}_\theta + \exp(j\pi/2)\vec{\underline{e}}_\phi] + d\ [\vec{\underline{e}}_\theta - \exp(j\pi/2)\vec{\underline{e}}_\phi] \qquad (2.56)$$

where c and d are complex quantities whose magnitudes are given by:

$$|c| = |E_\theta^{circl-pol}/2|(1 + m^2 + 2m\ \sin\Phi')^{1/2} \qquad (2.57)$$

$$|d| = |E_\theta^{circl-pol}/2|(1 + m^2 - 2m\ \sin\Phi')^{1/2} \qquad (2.58)$$

CHAPER III

COMPUTED RESULTS AND DISCUSSION

Based on the mathematical model developed in the previous chapter for the reflector, central blockage and the strut field, the expected reflector patterns for several cases has been computed. This chapter presents few selected data. A simplified feed model in the form of $\cos^m\theta$ ($\cos\theta$, $\cos^2\theta$) illumination is selected and the expected co-polar and cross-polar behaviours of different strut configurations are studied.

Since the cross-polarization will be higher for longer struts, only the case of struts mounted on the reflector edge are considered. For other cases the results can similarly be obtained, but the cross-polar components will be lower [1].

Three strut geometries are considered: a single strut, a tripod configuration and a quad-strut geometry. In all cases the struts are assumed to be located at an angle 45° with respect to the x'-y' plane and supported from the reflector edge, so that full plane wave blockage of the reflector exists. The reflector diameter, D, for all cases is kept at 48λ, with focal length to diameter ratio, $F/D = 0.375$, strut diameter, $2a = 0.5\lambda$ and the central blockage diameter, $2R_c = 2.5\lambda$, where λ is the wavelength.

3.1 Linearly Polarized Feed

For a single strut, with a y-polarized feed, the computed patterns are shown in Figures (3.1) to (3.4) for a cos θ feed pattern and in Figures (3.5) to (3.7) for a $\cos^2\theta$ feed pattern. The corresponding efficiencies are listed in Tables (3.1) and (3.2).

An examination of Figures (3.1) to (3.4) indicates that when the polarization of the feed is along the strut, the effect of the scattered field of the strut on the reflector pattern is larger. This is clear from Figure (3.3) where the level of the first sidelobe is higher and the overall reflector pattern has, generally, higher sidelobe levels than the pattern of Figure (3.1). The cross-polarization introduced by the struts is shown in Figures (3.2) and (3.4), which is quite satisfactory and is -54 dB level for the polarization along the strut while it is -54.5 dB, for the polarization perpendicular to the strut. Also, comparing the results of Table (3.1) it is clear that for the polarization along the strut, the blocked efficiency is lower; i.e. 80.196% compared with 80.342%.

Similar results are evident in Figures (3.5) to (3.7) for a $\cos^2\theta$ feed pattern. Again, when the feed polarization is along the strut, the blockage effect is higher and the corresponding blocked efficiency is lower, i.e., 68.88% compared with 70.0%. The cross-polarization has also similar behaviour, with a peak level about -53 dB.

Comparing the results of two different illuminations, we note that as expected, for a $\cos^2\theta$ feed pattern the effect of the blockage is very significant. In fact, when the feed polarization is perpendicular to the strut, the main pattern deterioration is due to the central blockage. The struts have a minimal effect. For struts along the feed polarization, the effect of the strut in the plane normal to the strut is very high and of the same order as the central blockage effect. For a cos θ illumination both central and strut blocking have negligible effect on the reflector pattern. From these results we conclude that, although by strong tapering of the feed illumination ($\cos^2\theta$ feed), sidelobe levels can be lowered to around -38 dB. The aperture blockage raises their level to about -30 dB. In the case of cos θ illumination the original sidelobe level of about -25 dB increases to around -23 dB level.

For identical feed and strut dimensions the computed results for a tripod configuration are shown in Figures (3.8) to (3.13). The polarization of the field is along the y-direction. From Figures (3.8) to (3.10) again it is evident that blockage effect on the reflector pattern is small for a cos θ feed pattern. In fact, provided that the struts are not along the E-plane the blockage effect of a tripod on the sidelobes, seems to be smaller than that of a single strut along the feed polarization. The blockage efficiency however is lower; i.e., 78.33% compared to 80.196%. The cross polarization is also poor which is indicated in Figures (3.9) and (3.10) and has a maximum level of about -41 dB. Similar results are also obtained for a $\cos^2\theta$ illumination, which are shown in Figues (3.11) to (3.13). Sidelobe performance is satisfactory and increase their level slightly above that of the central blockage. The first sidelobe is about -32 dB. A major disadvantage of a tripod configuration is the generally high level of the higher order sidelobes, which although are lower than those of a single strut located along the E-plane their level is otherwise higher. The computed efficiences, for this configuration are shown in Tables (3.3) and (3.4). They are, as expected, lower than those of a single strut and for two assumed illuminations are 78.33% and 67.06% respectively.

Figures (3.14) to (3.17) show the computed patterns for a quad-configuration. Again, the dimensions of the feed and struts are the same as before and strut lengths are assumed to be the full length of the aperture. Furthermore, for the computed data two struts are assumed along the feed polarization. Therefore, the sidelobe levels, indicated in these figures, are the maximum levels that one generally should expect. Deterioration of the pattern in the principle E-plane is most severe for higher order sidelobes, but the cross-polarization is satisfactory at about -52 dB. The computed efficiencies are shown in Tables (3.5) and (3.6).

To indicate the effect of strut diameter on the reflector pattern Figures (3.18) and (3.19) are also included, which are respectively for tripod and quad-strut configurations. In both cases the strut diameter has been increased to one λ and the illuminations due to a cos θ feed pattern. For the tripod geometry the level of the first sidelobe is almost unaffected, odd sidelobe levels have been reduced and the even sidelobes are raised. For a quad-strut case, in Figure (3.19), the shape of the pattern has remained the same, but its level has increased almost uniformly. It is therefore clear that the diameter of the strut has a strong effect on the pattern of a quad configuration, but generally does not affect the results of a tripod geometry. Corresponding efficiencies are shown in Table (3.7), which indicate lower percentages than those for a 0.5λ strut.

3.2 Circularly Polarized Feed

Performance of the symmetric reflector with a circularly polarized feed is also studied. For the same reflector, feed and strut dimensions, the radiation patterns for the unblocked reflector and both of the three strut geometries are computed and the results are shown in Figures (3.20) to (3.25) for a cos θ feed pattern. The co-polar and cross-polar pattens may be compared with those of a y-polarized feed.

For an unblocked reflector, Figure (3.20), the co-polar radiation pattern is exactly the same as that of a y-polarized feed. But, while the cross-polarization is typically zero for a y-polarized feed, it has a value of -54 dB for a circularly-polarized feed.

For a single strut, with a circularly- polarized feed, the computed patterns are shown in Figures (3.21) and (3.24). An examination of these two figures shows that the co-polar patterns are exactly the same as those of the corresponding configuration with a y-polarized feed. At $\phi = 45°$, the cross-polarization level is about -45 dB compared with -54 dB for a y-polarized feed while at $\phi = 0$ the cross polarization level is still about -45 dB, compared with an approximately vanishing value in the case of a y-polarized feed.

For a tripod configuration the co-polar and cross-polar radiation patterns at ϕ = 60° and ϕ = 120°, with a circularly-polarized cos θ feed, are exactly the same as the corresponding patterns obtained in the case of a y-polarized feed and have not been presented again. At ϕ = 0, the co-polar and cross-polar patterns are the same as those computed at ϕ = 120°. This means that the cross-polarization level at ϕ = 0 (-41 dB) is higher than that at ϕ = 60° (-43 dB).

For a quad configuration and at ϕ =45° plane, the co-polar and the cross-polarization patterns are exactly the same for both circular and y-polarized feeds and have not been presented again. They are very nearly the same as those of the unblocked reflector. Thus the struts have a minimal effect in this case. At ϕ = 0, the co-polar and the cross-polar patterns are shown in Figure (3.25). The sidelobe levels are somewhat lower than those obtained in the case of a y-polarized feed. On the other hand, the cross-polarization level is very high (-37.5 dB) compared with approximately vanishing value of the y-polarized case. At ϕ = 90°, the obtained patterns are exactly the same as those of ϕ = 0 case.

From the above results we see that the co-polar patterns of the symmetric reflector with a circularly polarized feed are either similar or very near (with a somewhat lower sidelobe levels) to the co-polar patterns of a y-polarized feed. The cross-polarization levels are either equal to or somewhat higher than those of a y-polarized feed. Except in the principal planes where the cross-polarization levels of the circularly-polarized feed are generally very high compared with an approximately vanishing value for a y-polarized feed. It is also seen that in the case of a quad-strut configuration, the struts have a minimal effect on the reflector radiation pattern.

TABLE 3.1

Efficiencies of a Single Strut

Feed Diameter = 2.5λ,

Strut Diameter = 0.5λ, Reflector Diameter = 48 λ, cos θ Illumination

Spillover power	5.69%
Unblocked efficiency η_0	82.803%
Unblocked gain G_o	42.75 dB
Blocked efficiency η_B	
(i) Strut Perpendicular to the E-plane	81.342%
(ii) Strut Along the E-plane	80.196%
Blocked gain G_B	
(i) Strut Perpendicular to the E-plane	42.67 dB
(ii) Strut Along the E-plane	42.61 dB

TABLE 3.2

Efficiencies of a Single Strut

Dimensions Same as Table 3.1, $\cos^2\theta$ Illumination

Spillover power	0.84%
Unblocked efficiency η_0	71.61%
Unblocked gain G_o	42.12 dB
Blocked efficiency η_B	
(i) Strut Perpendicular to the E-plane	70.0%
(ii) Strut Along the E-plane	68.88%
Blocked gain G_B	
(i) Strut Perpendicular to the E-plane	42.02 dB
(ii) Strut Along the E-plane	41.95 dB

TABLE 3.3

Efficiencies of a Tripod

Dimensions Same as Table 3.1, cos θ Illumination

Spillover power	5.69%
Unblocked efficiency η_o	82.803%
Unblocked gain G_o	42.75 dB
Blocked efficiency η_B	78.33%
Blocked gain G_B	42.51 dB

TABLE 3.4

Efficiencies of a Tripod

Dimensions Same as Table 3.1, $\cos^2\theta$ Illumination

Spillover power	0.84%
Unblocked efficiency η_o	71.61%
Unblocked gain G_o	42.12 dB
Blocked efficiency η_B	67.06%
Blocked gain G_B	41.83 dB

TABLE 3.5

Efficiencies of a Quad-Strut

Dimensions Same as Table 3.1, cos θ Illumination

Spillover power	5.69%
Unblocked efficiency η_o	82.80%
Unblocked gain G_o	42.75 dB
Blocked efficiency η_B	77.12%
Blocked gain G_B	42.44 dB

TABLE 3.6

Efficiencies of a Quad-Strut

Dimensions Same as Table 3.1, $\cos^2\theta$ Illumination

Spillover power	0.84%
Unblocked efficiency η_o	71.61%
Unblocked gain G_o	42.12 dB
Blocked efficiency η_B	65.89%
Blocked gain G_B	41.76 dB

TABLE 3.7

Efficiencies of a Tripod and a Quad,
Feed Diameter = 2.5λ, Strut Diameter = 1.0λ,
Reflector Diameter = 48λ, cos θ Illumination

Spillover power	5.69%
Unblocked efficiency η_o	82.80%
Unblocked gain G_o	42.75 dB
Blocked efficiency η_B	
(i) A Tripod	74.7%
(ii) A Quad	72.34%
Blocked gain G_B	
(i) A Tripod	42.3 dB
(ii) A Quad	42.16 dB

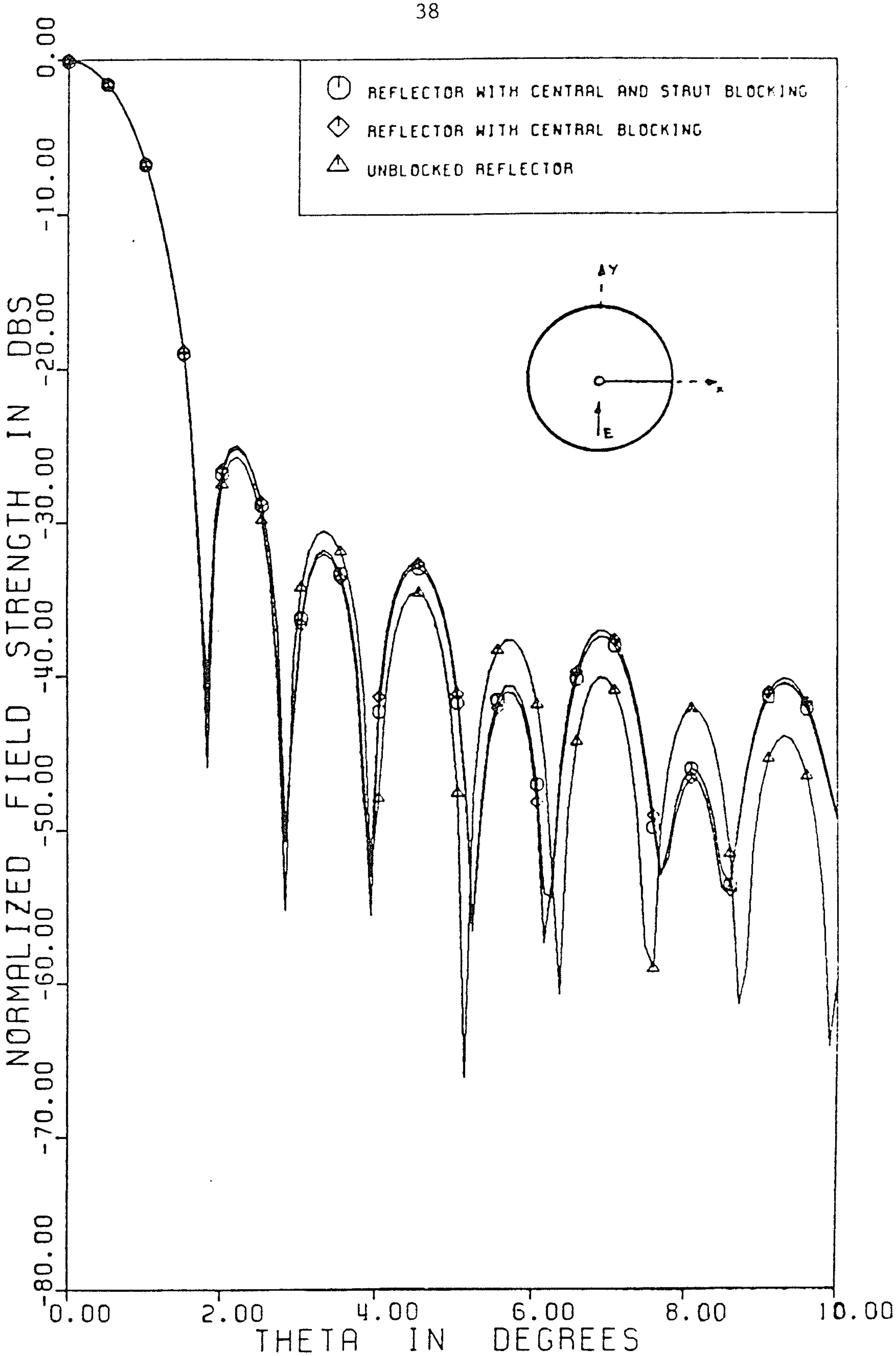

Figure 3.1. Single strut co-polar patterns with cos θ illumination , $\phi = 0^0$ plane , a = 0.25 λ , y - polarization .

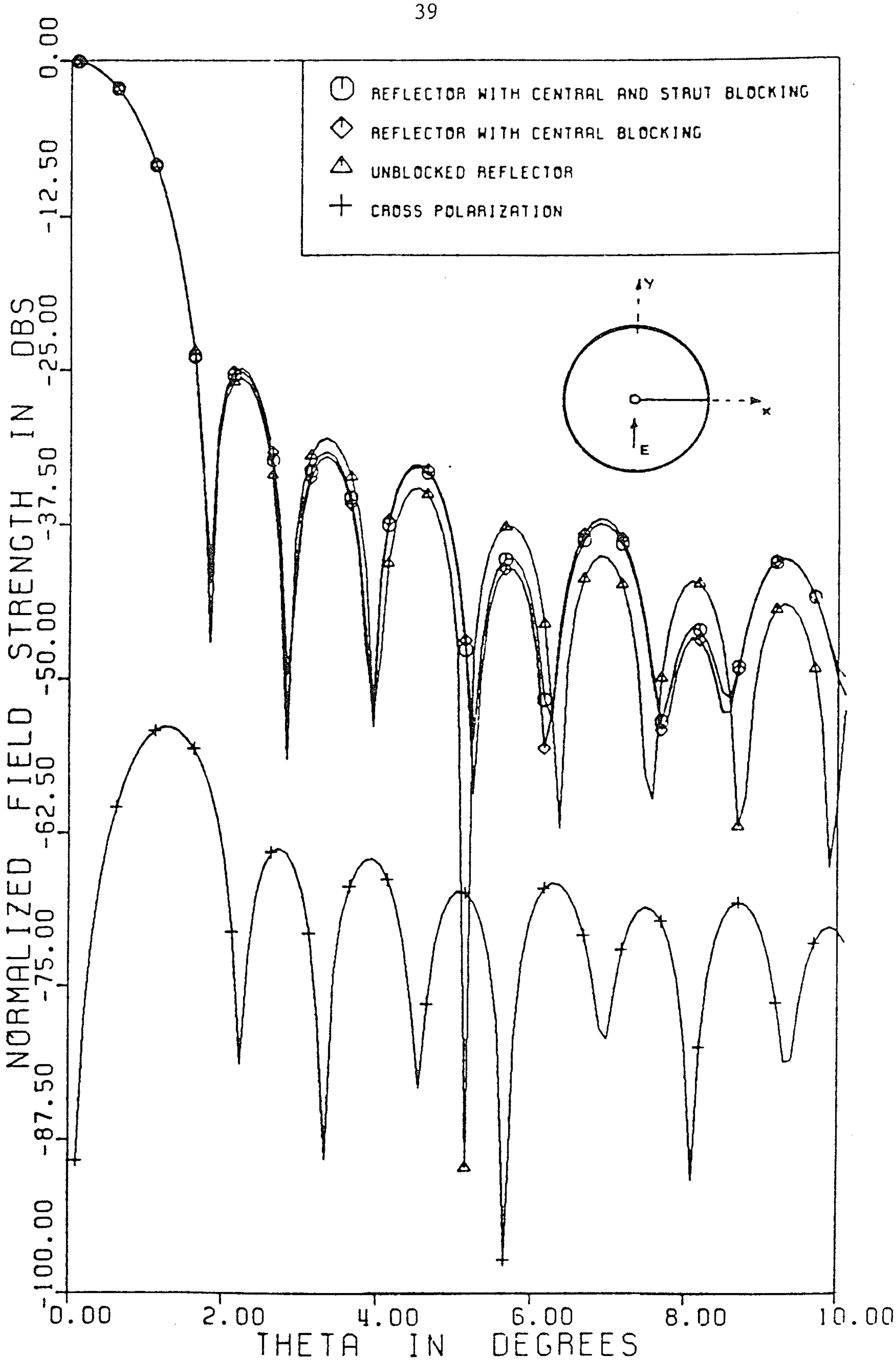

Figure 3.2. Single strut co-polar and cross - polar patterns with cos θ illumination , $\phi = 45^0$ plane , a =0.25 λ , y - polarization .

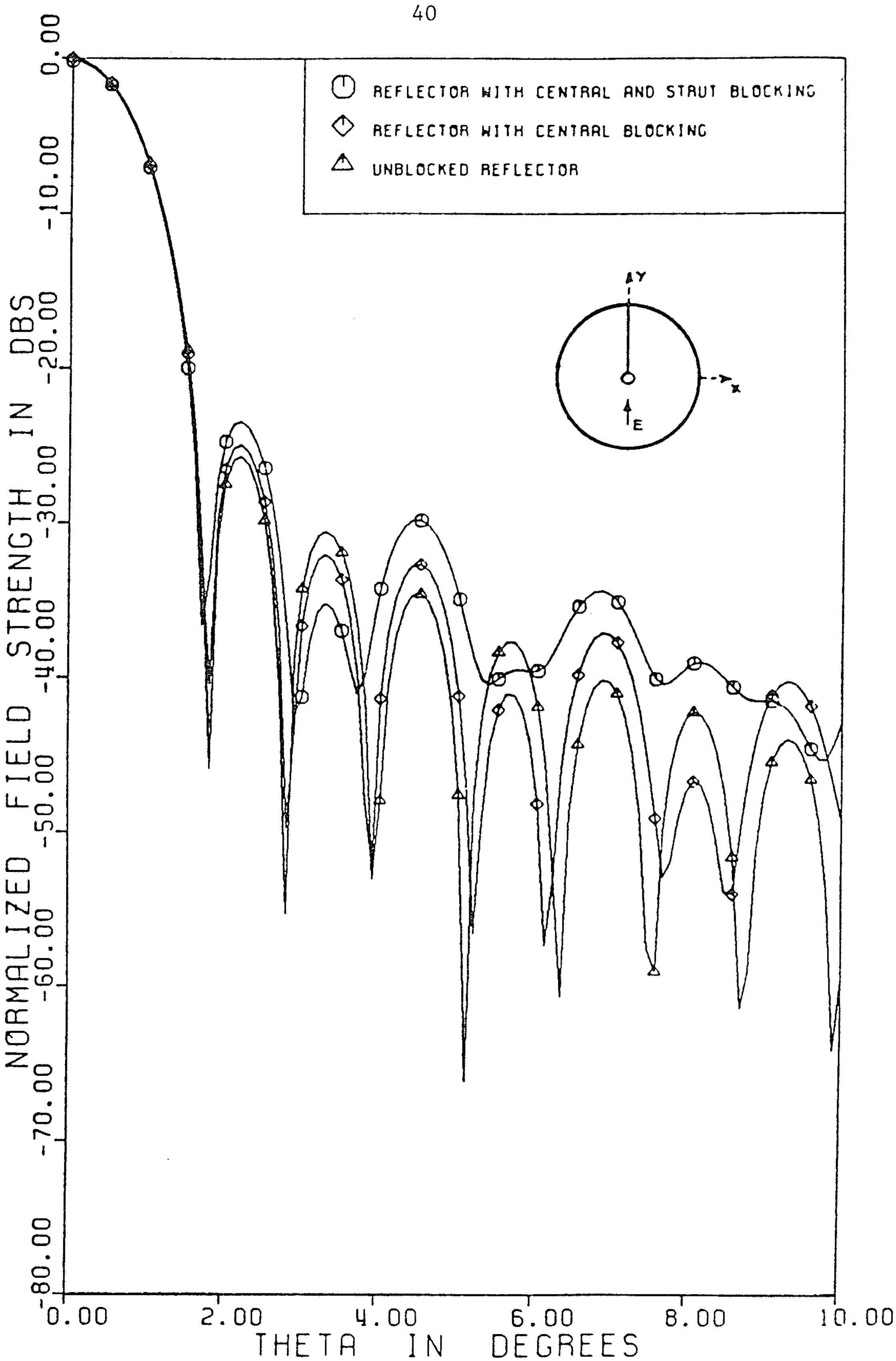

Figure 3.3. Single strut co-polar patterns with cos θ illumination , $\phi = 0^0$ plane , a = 0.25 λ , y - polarization .

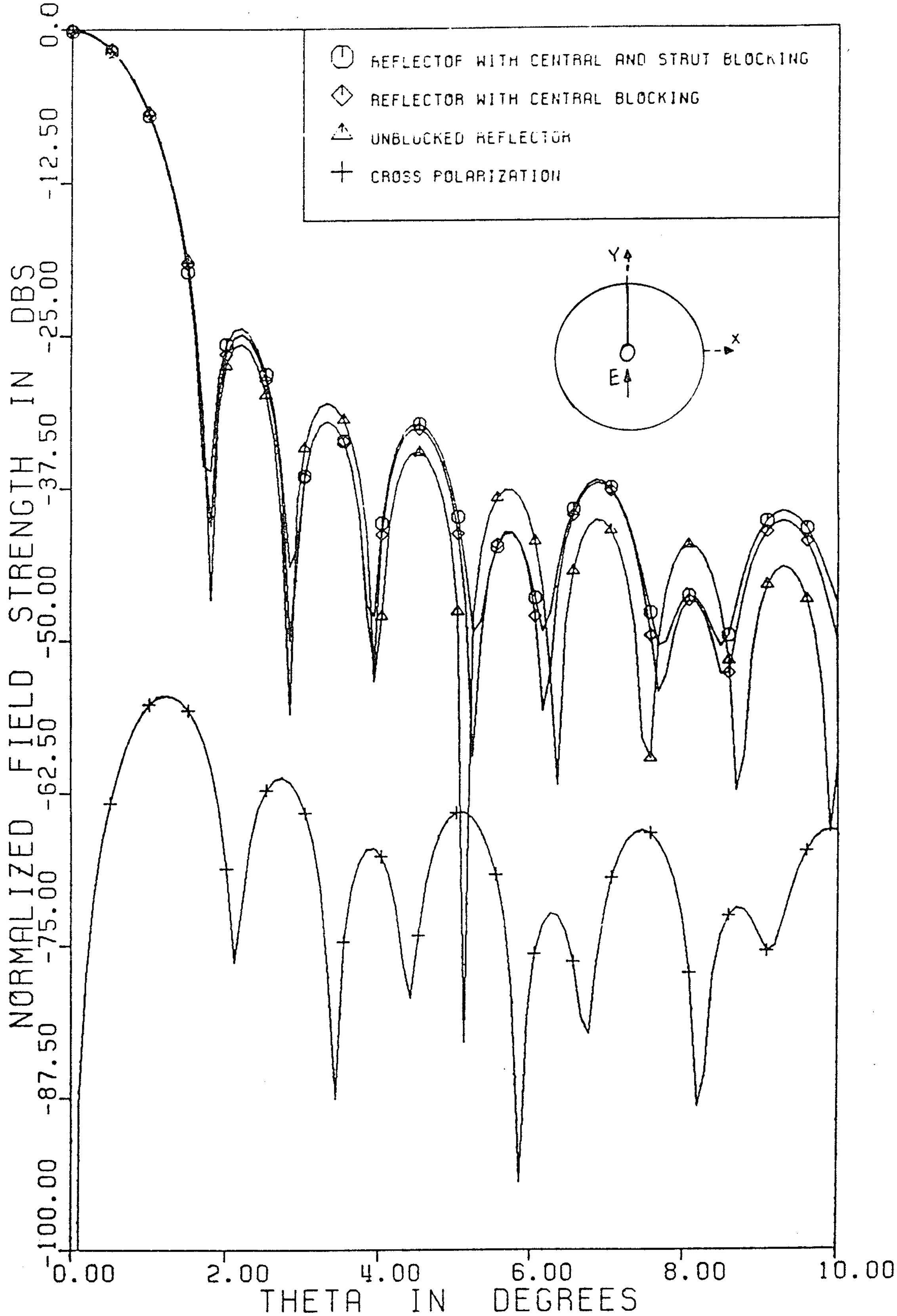

Figure 3.4. Single strut co-polar and cross - polar patterns with cos θ illumination , $\phi = 45^0$ plane , a = 0.25 λ , y - polarization .

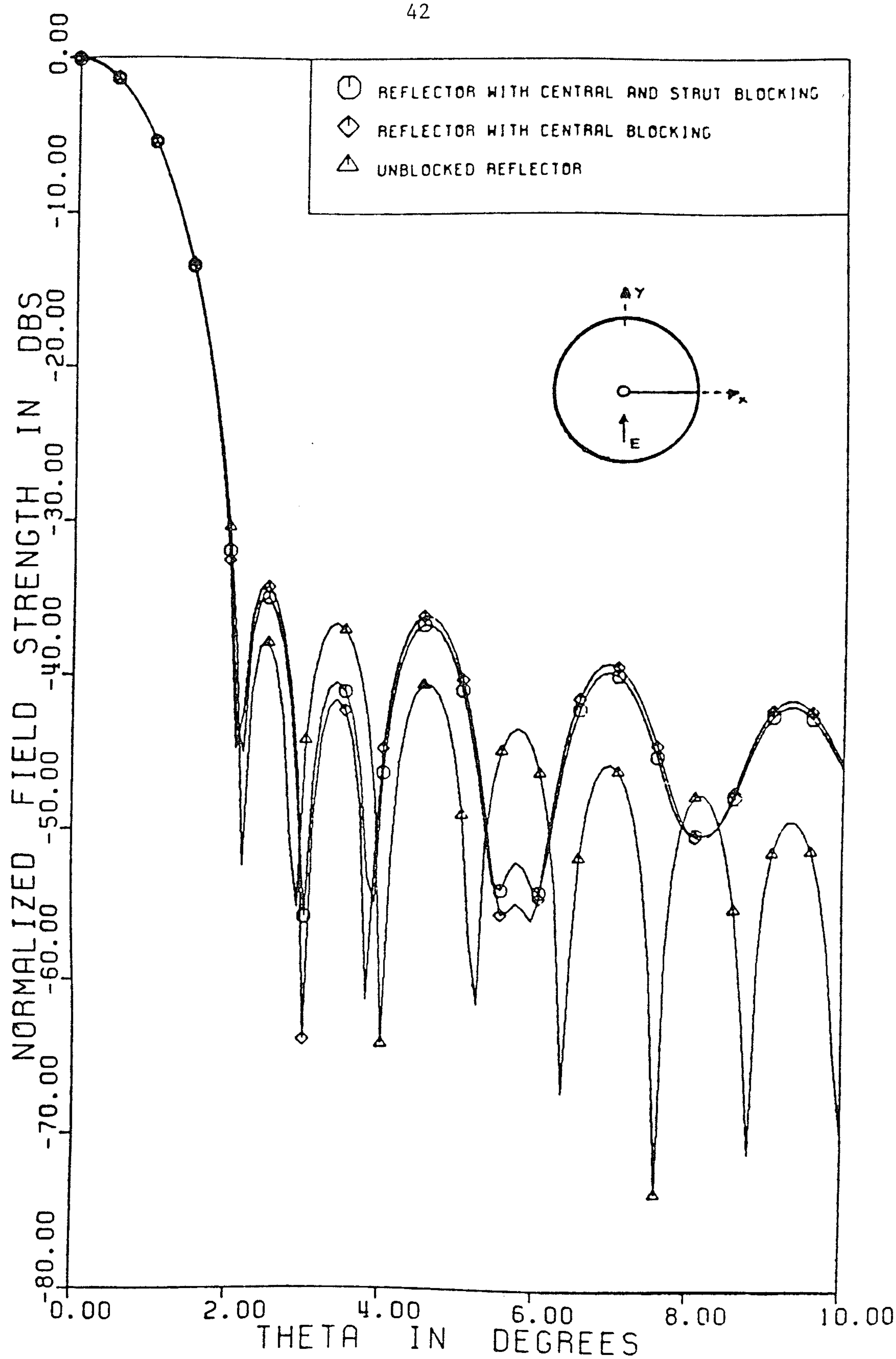

Figure 3.5. Single strut co-polar patterns with $\cos^2 \theta$ illumination, $\phi = 0^0$ plane, $a = 0.25\ \lambda$, y - polarization.

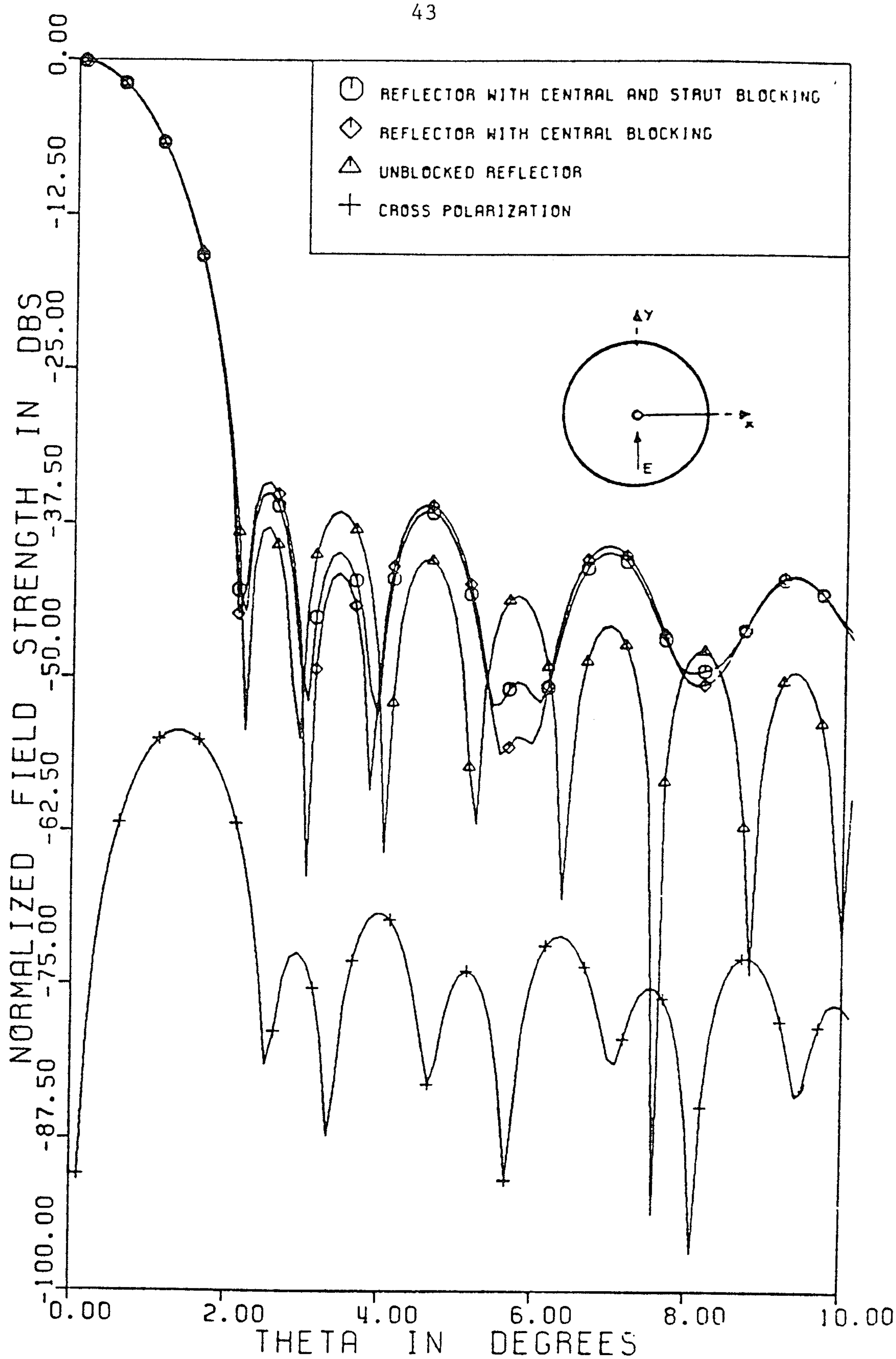

Figure 3.6. Single strut co-polar and cross - polar patterns with $\cos^2 \theta$ illumination , $\phi = 45^0$ plane , $a = 0.25\ \lambda$, y - polarization .

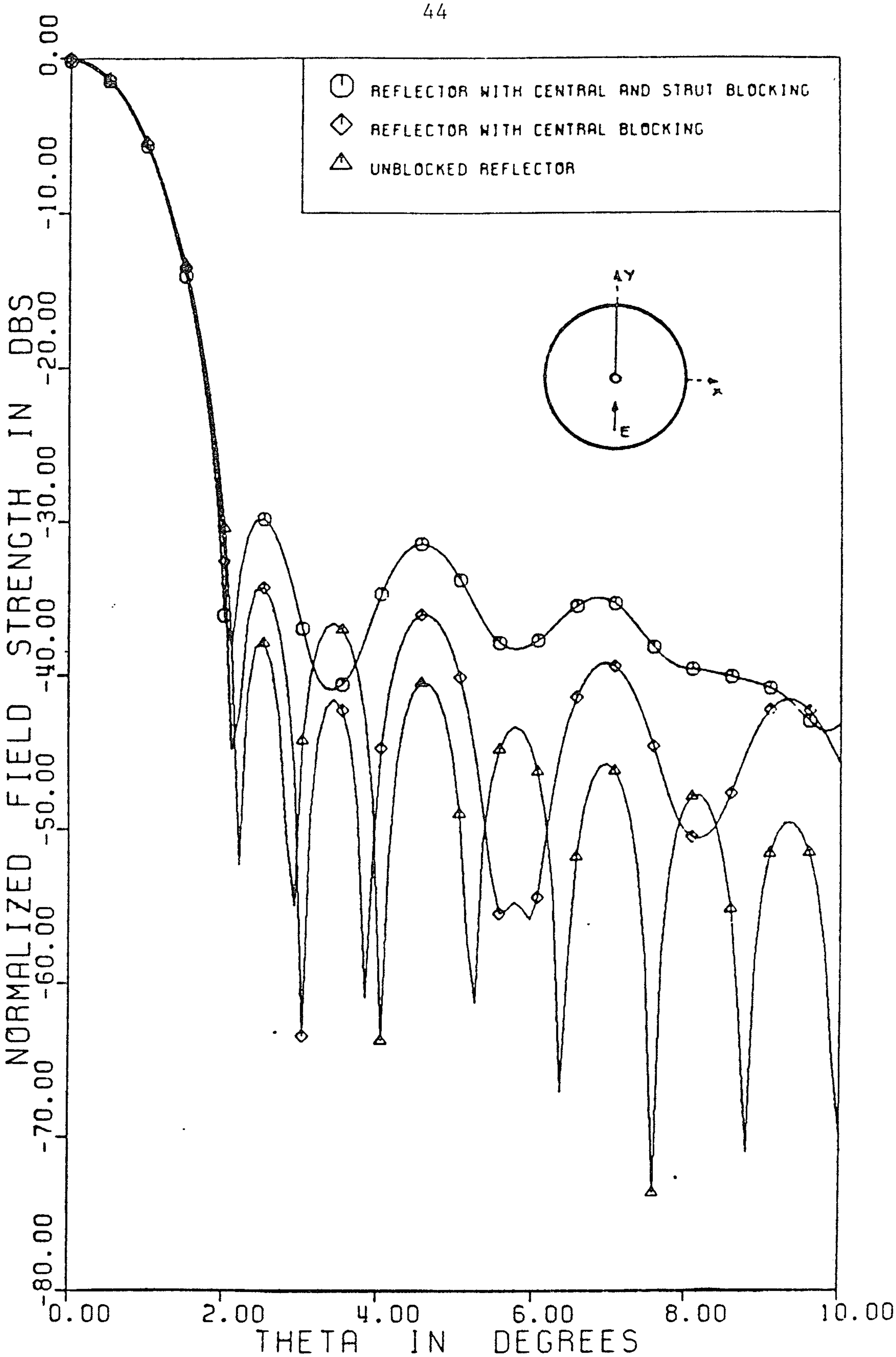

Figure 3.7. Single strut co-polar patterns with $\cos^2\theta$ illumination, $\phi = 0^0$ plane, $a = 0.25\,\lambda$, y - polarization.

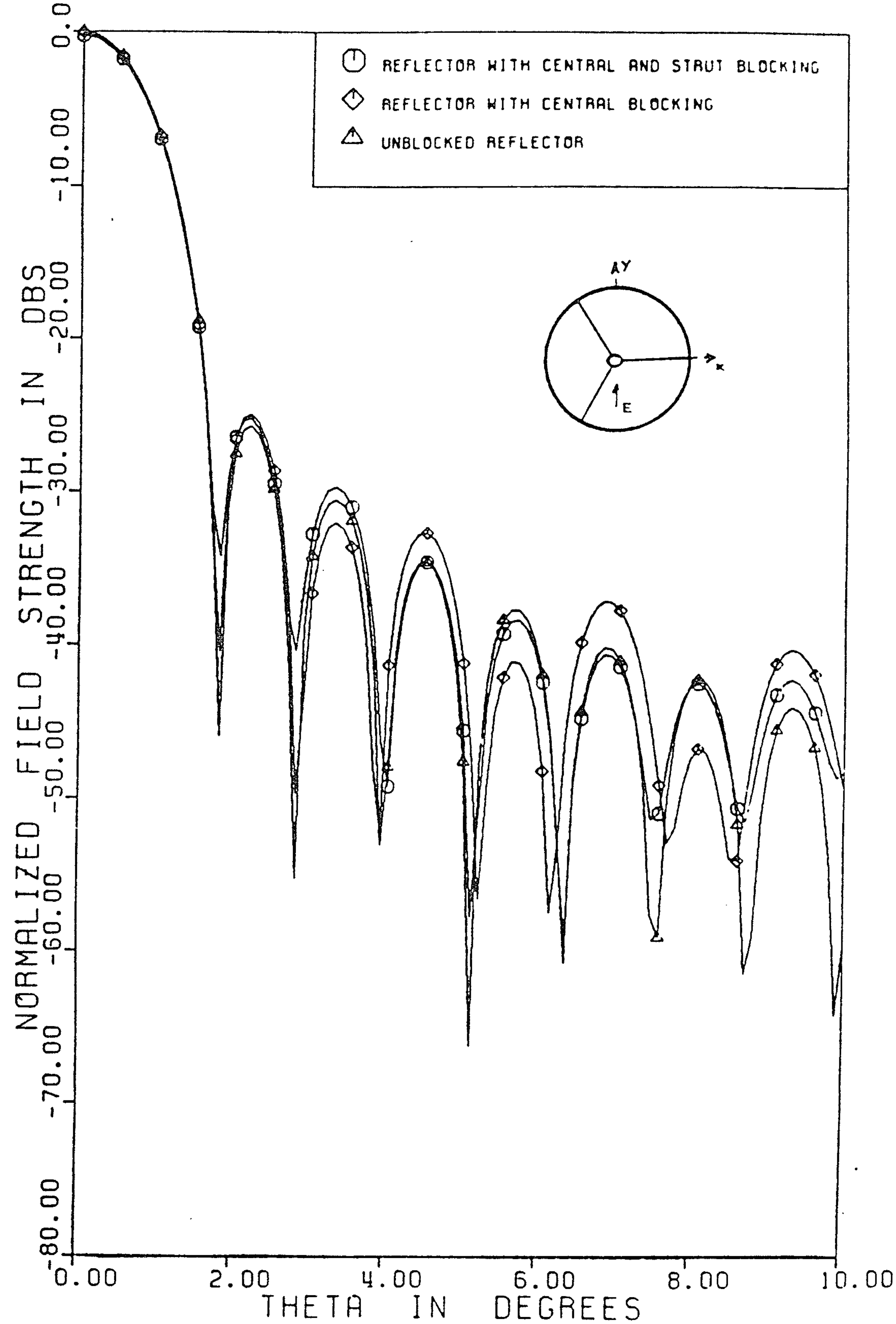

Figure 3.8. Tripod co-polar patterns with cos θ illumination , $\phi = 0^0$ plane , $a = 0.25\ \lambda$, y - polarization .

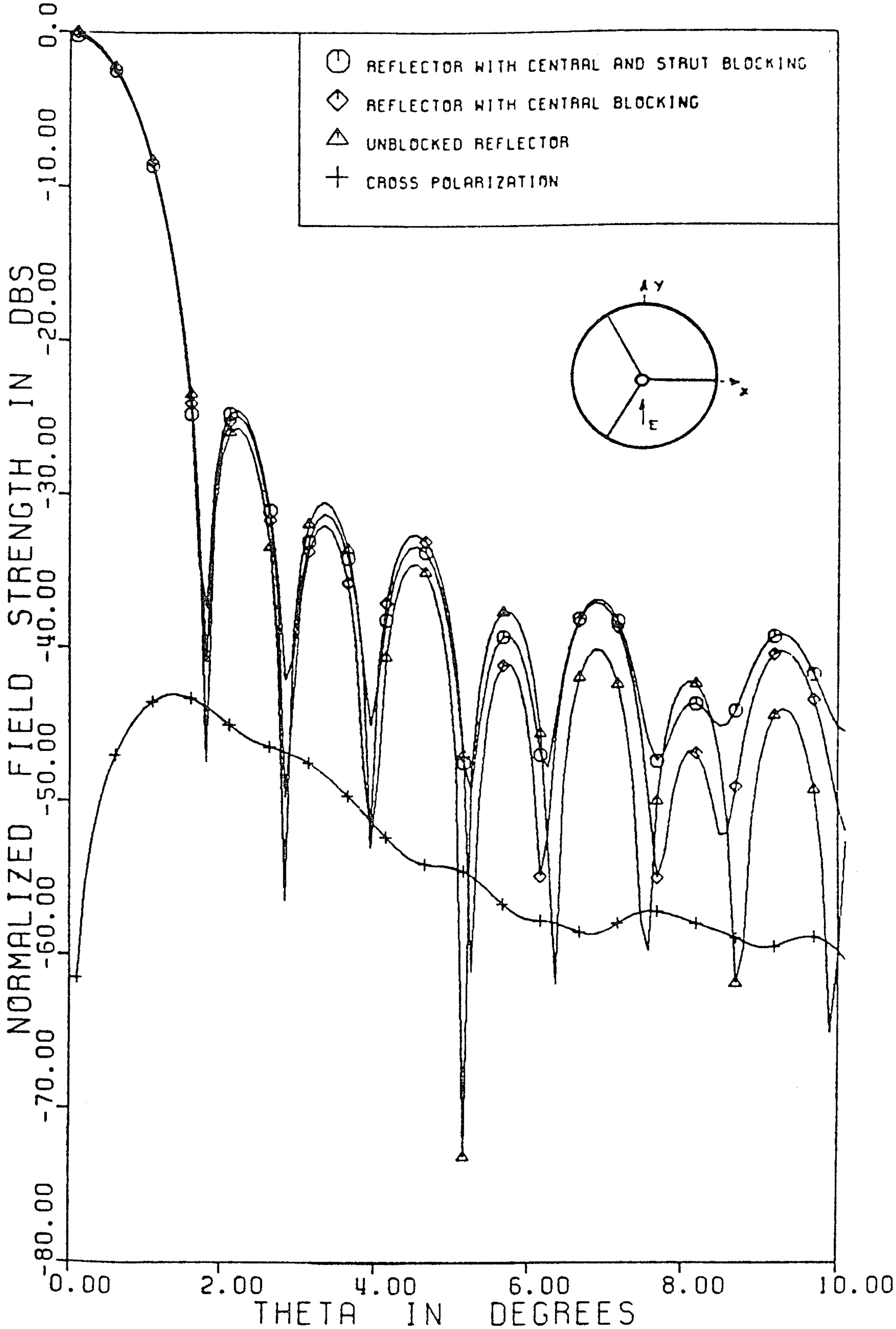

Figure 3.9. Tripod co-polar and cross - polar patterns with cos θ illumination , $\phi = 60^0$ plane ,a = 0.25 λ , y - polarization .

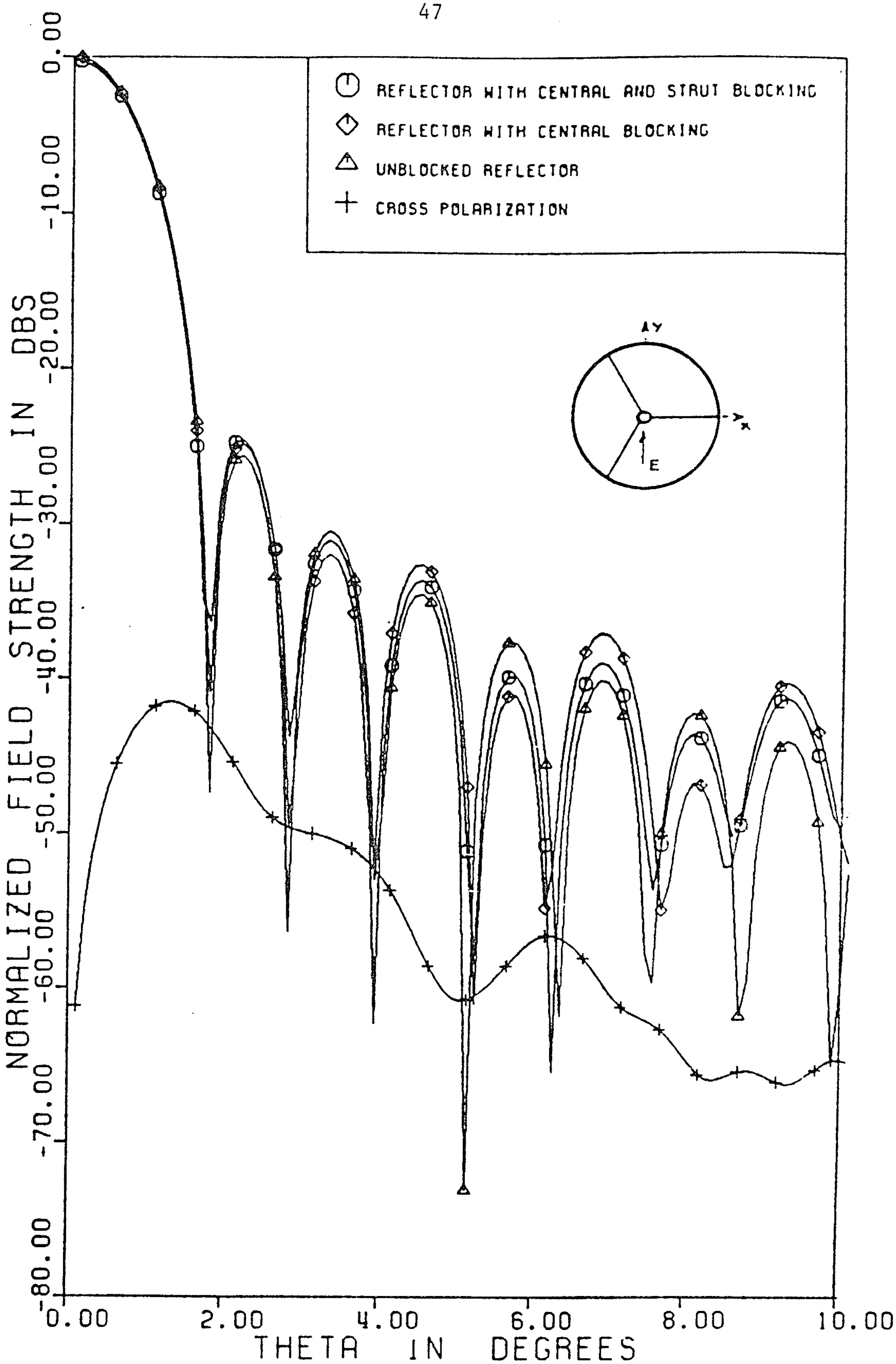

Figure 3.10. Tripod co-polar and cross - polar patterns with cos θ illumination , $\phi = 120^0$ plane , $a = 0.25\ \lambda$, y - polarization .

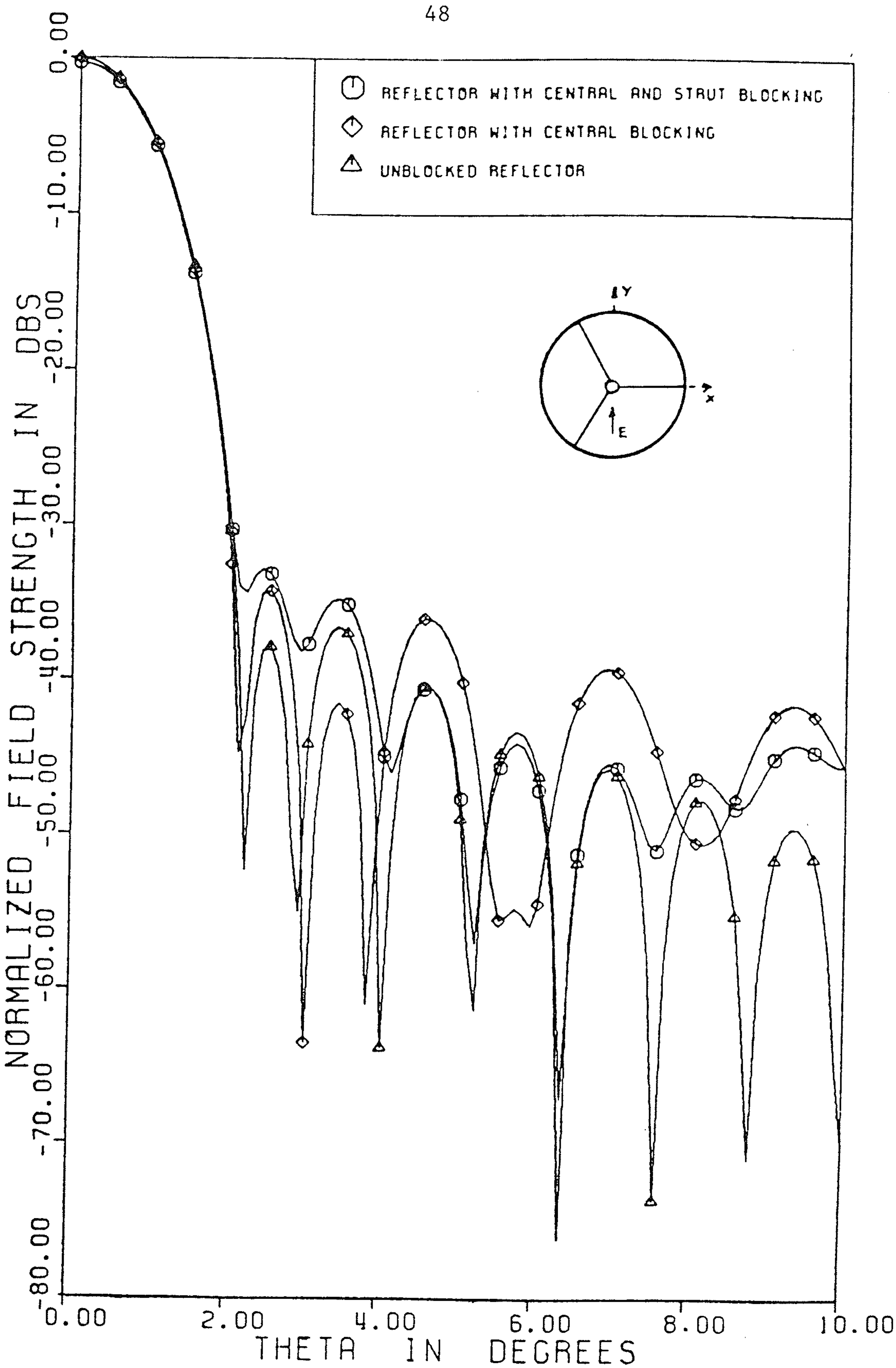

Figure 3.11. Tripod co-polar and cross - polar patterns with $\cos^2 \theta$ illumination , $\phi = 0^0$ plane , $a = 0.25\ \lambda$, y - polarization .

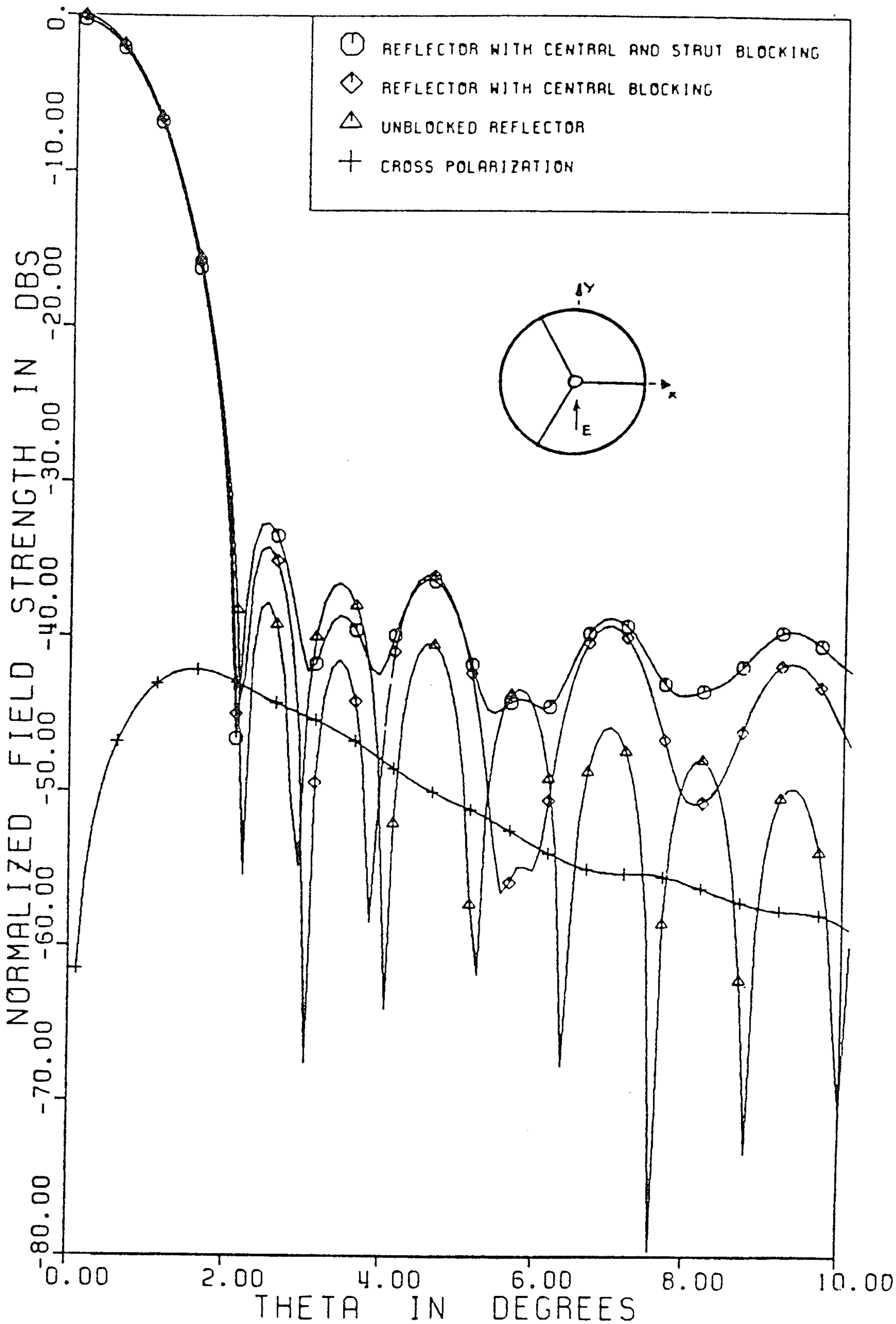

Figure 3.12. Tripod co-polar and cross - polar patterns with $\cos^2\theta$ illumination , $\phi = 60^0$ plane , $a = 0.25\ \lambda$, y - polarization .

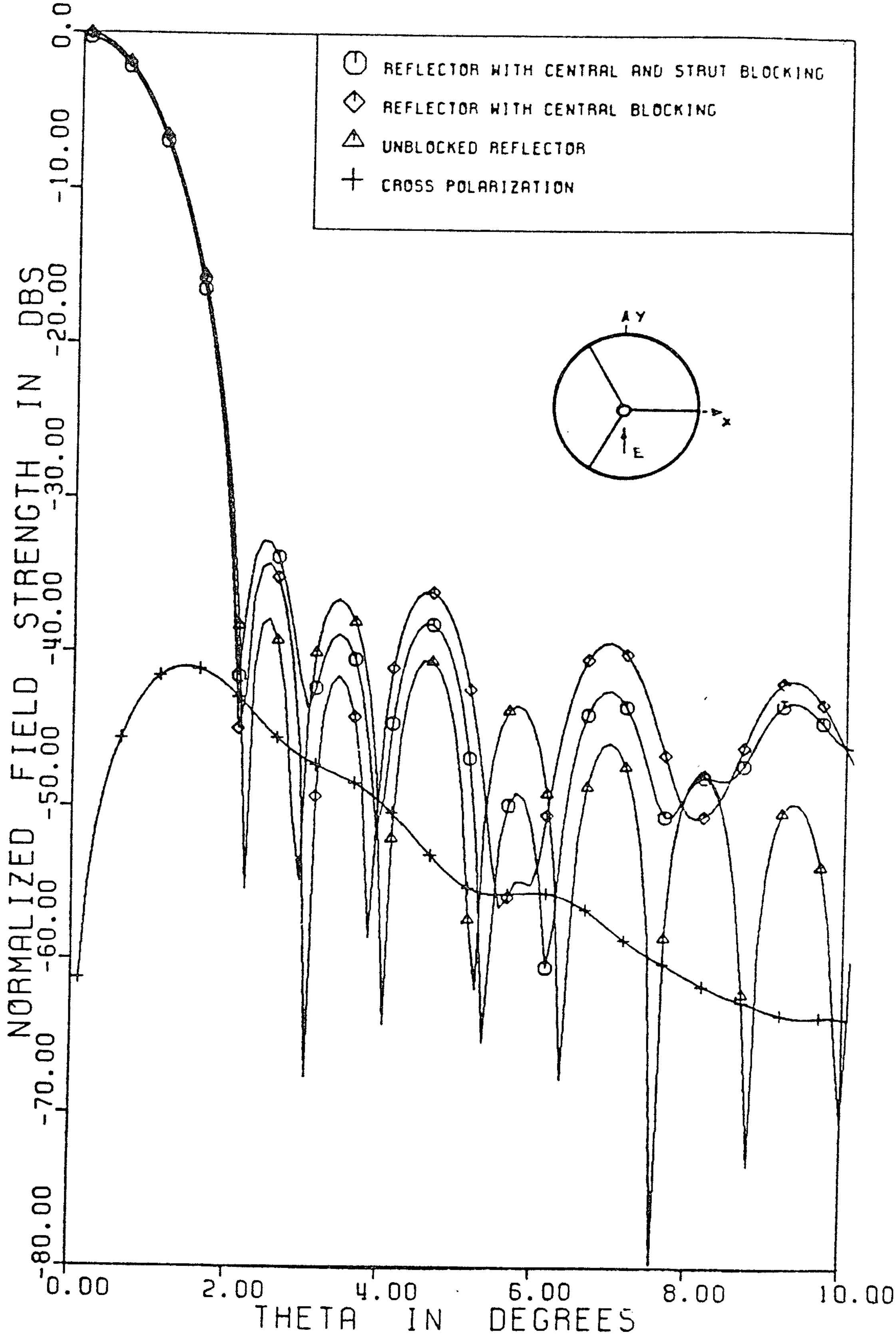

Figure 3.13. Tripod co-polar and cross - polar patterns with $\cos^2 \theta$ illumination , $\phi = 120^0$ plane , $a = 0.25\ \lambda$, y - polarization .

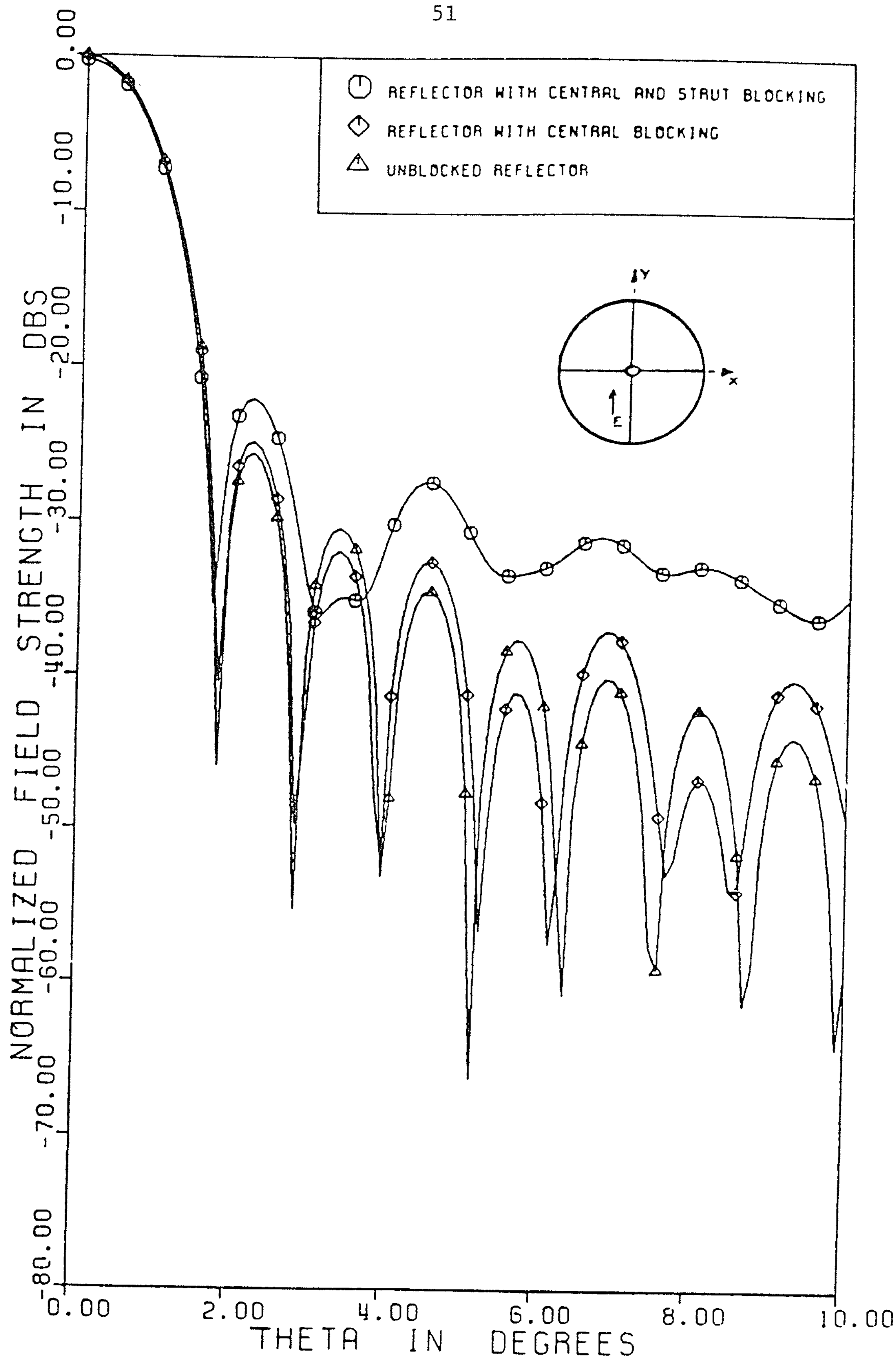

Figure 3.14. Quad co-polar patterns with cos θ illumination , ϕ = 0° plane , a = 0.25 λ , y - polarization .

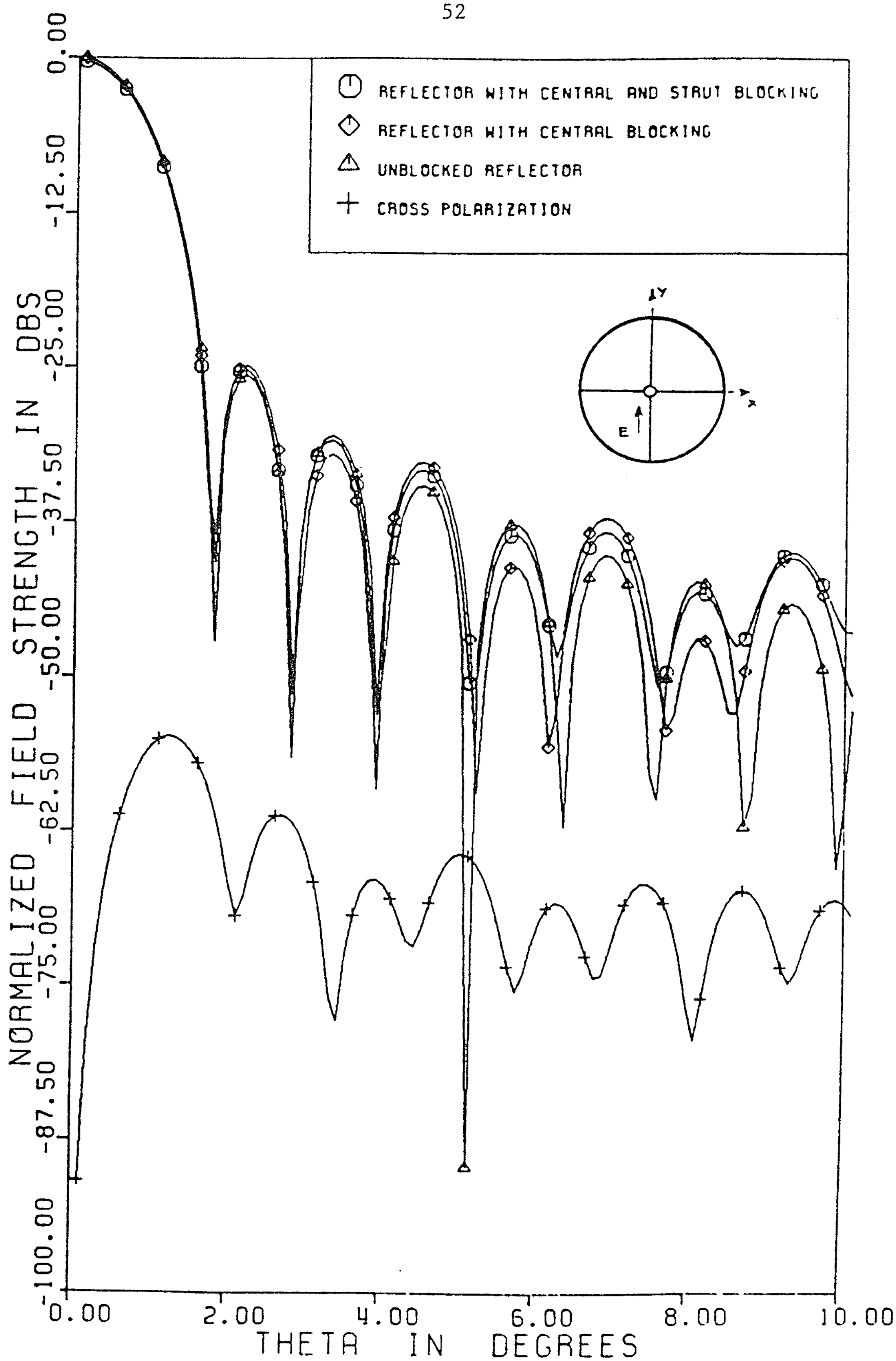

Figure 3.15. Quad co-polar and cross - polar patterns with cos θ illumination , $\phi = 45^0$ plane , $a = 0.25\ \lambda$, y - polarization .

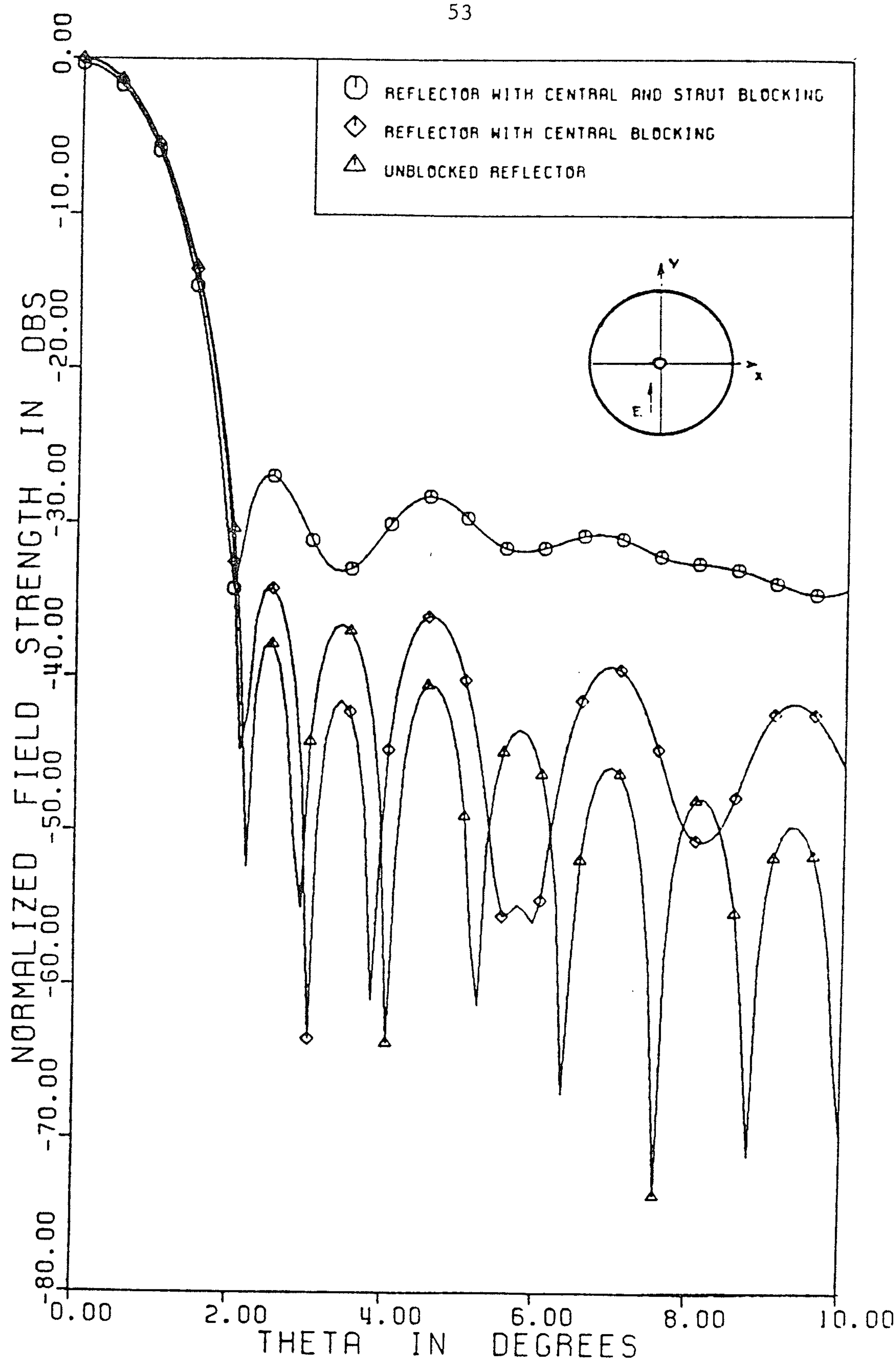

Figure 3.16. Quad co-polar patterns with $\cos^2\theta$ illumination , $\phi = 0^0$ plane , a = 0.25 λ , y - polarization .

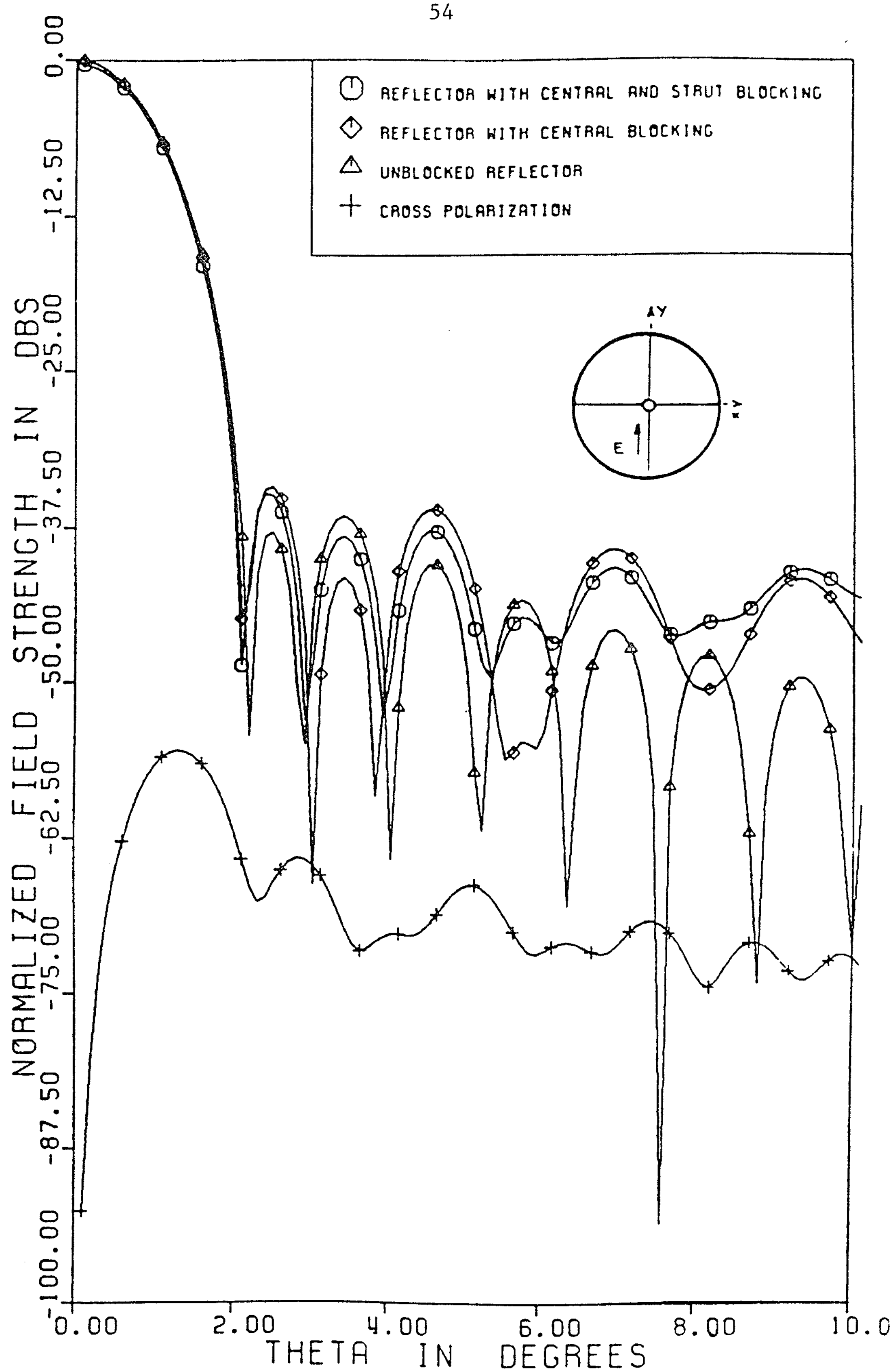

Figure 3.17. Quad co-polar and cross - polar patterns with $\cos^2 \theta$ illumination , $\phi = 45^0$ plane , $a = 0.25\ \lambda$, y - polarization .

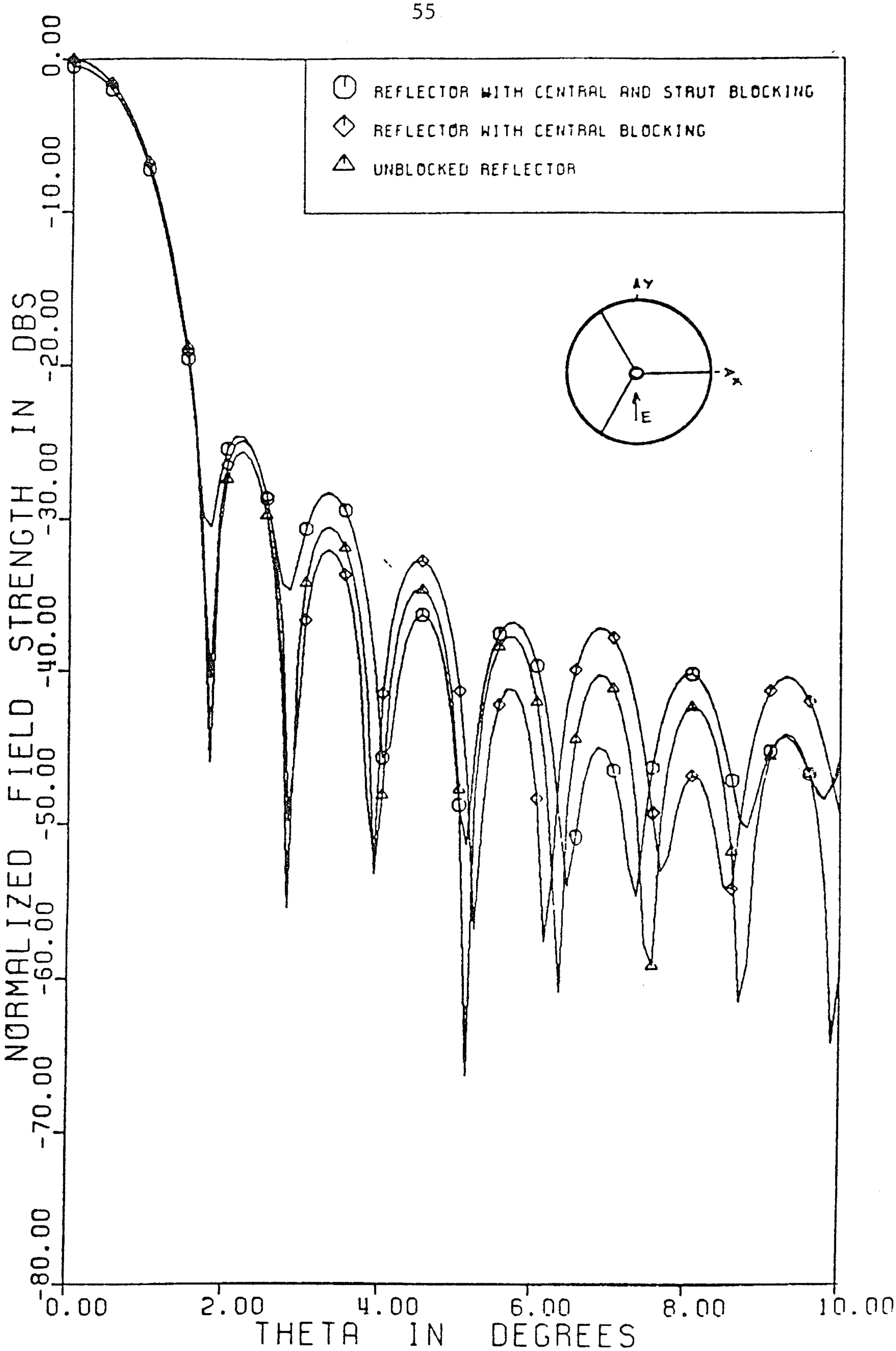

Figure 3.18. Tripod co-polar patterns with cos θ illumination , $\phi = 0^0$ plane , $a = 0.5\ \lambda$, y - polarization .

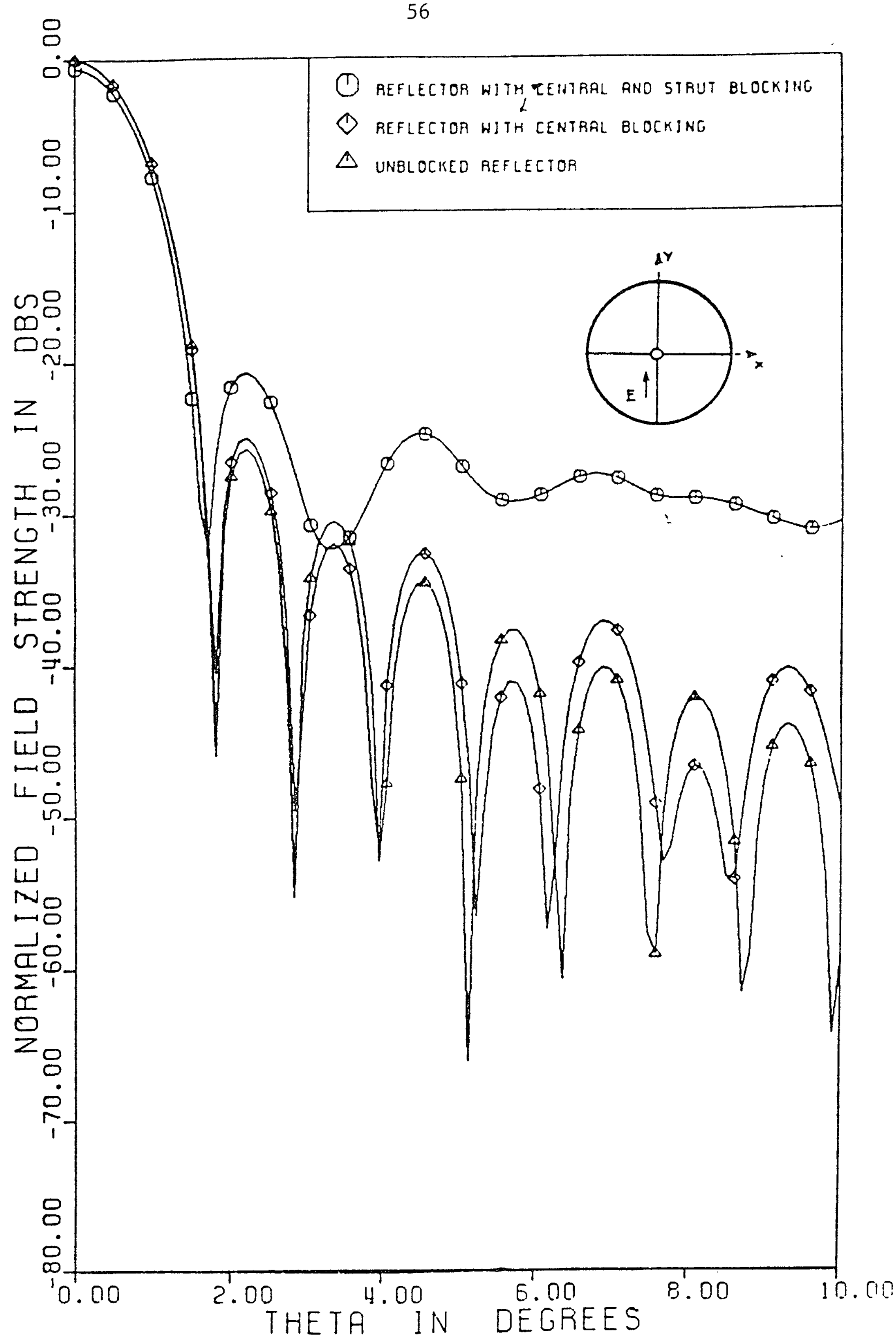

Figure 3.19. Quad co-polar pattern with cos θ illumination , $\phi = 0^0$, $a = 0.5\ \lambda$, y - polarization .

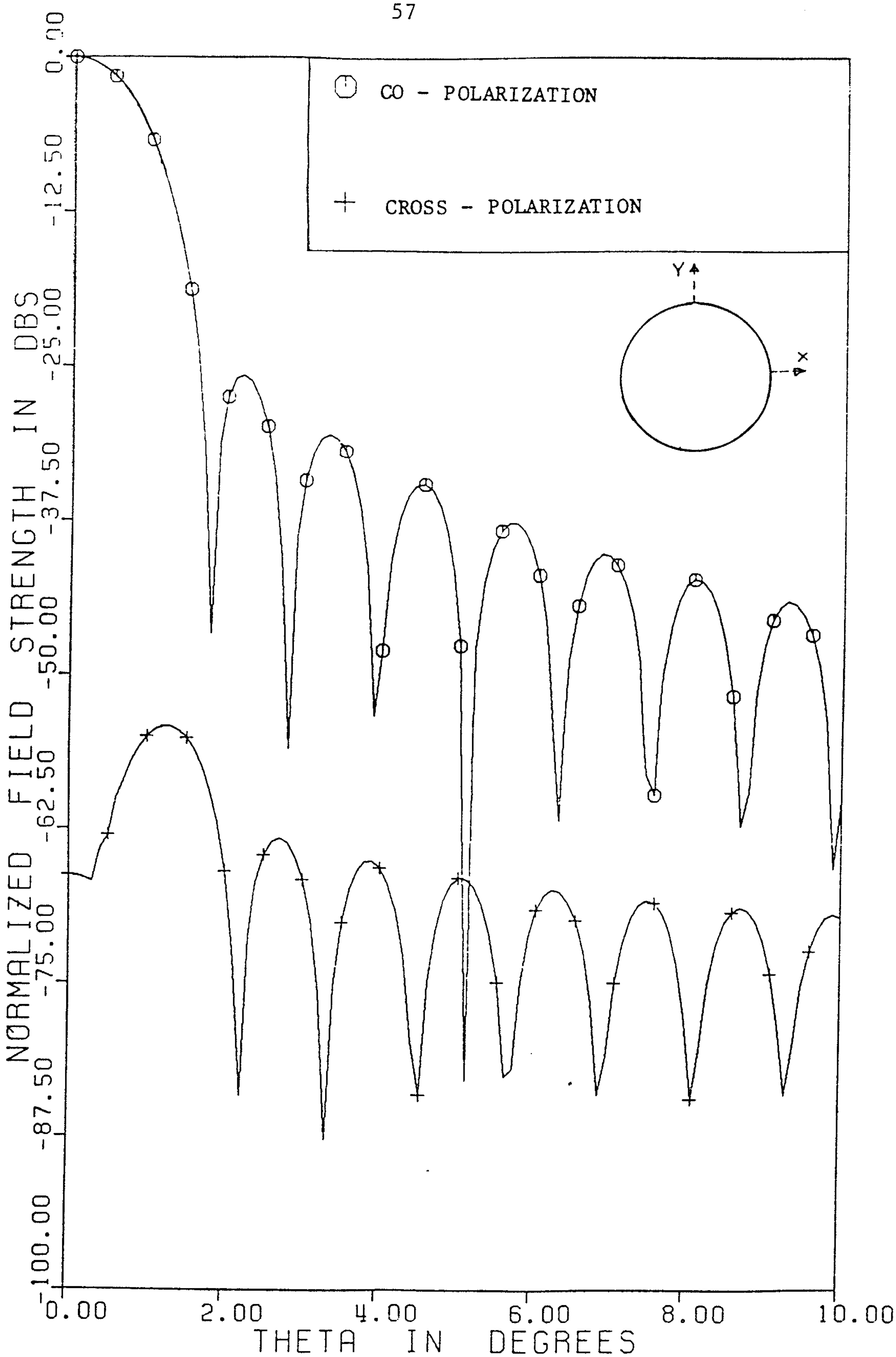

Figure 3.20. Unblocked reflector co-polar and cross - polar patterns of a circular polarization feed with a cos θ illumination .

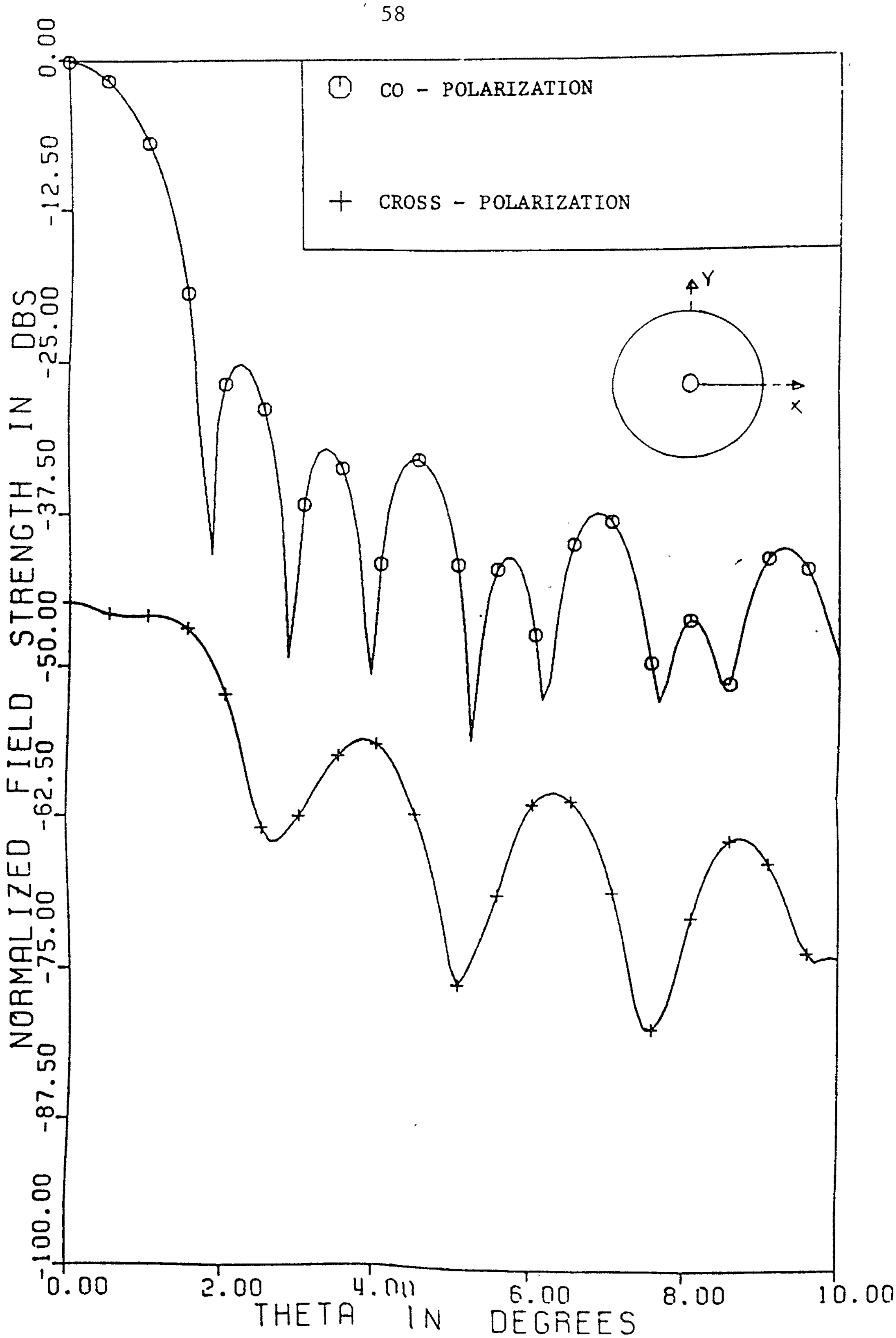

Figure 3.21. Single strut co-polar and cross - polar patterns of a circular polarization feed with a cos θ illumination , $\phi = 0^0$, $a = 0.25\ \lambda$.

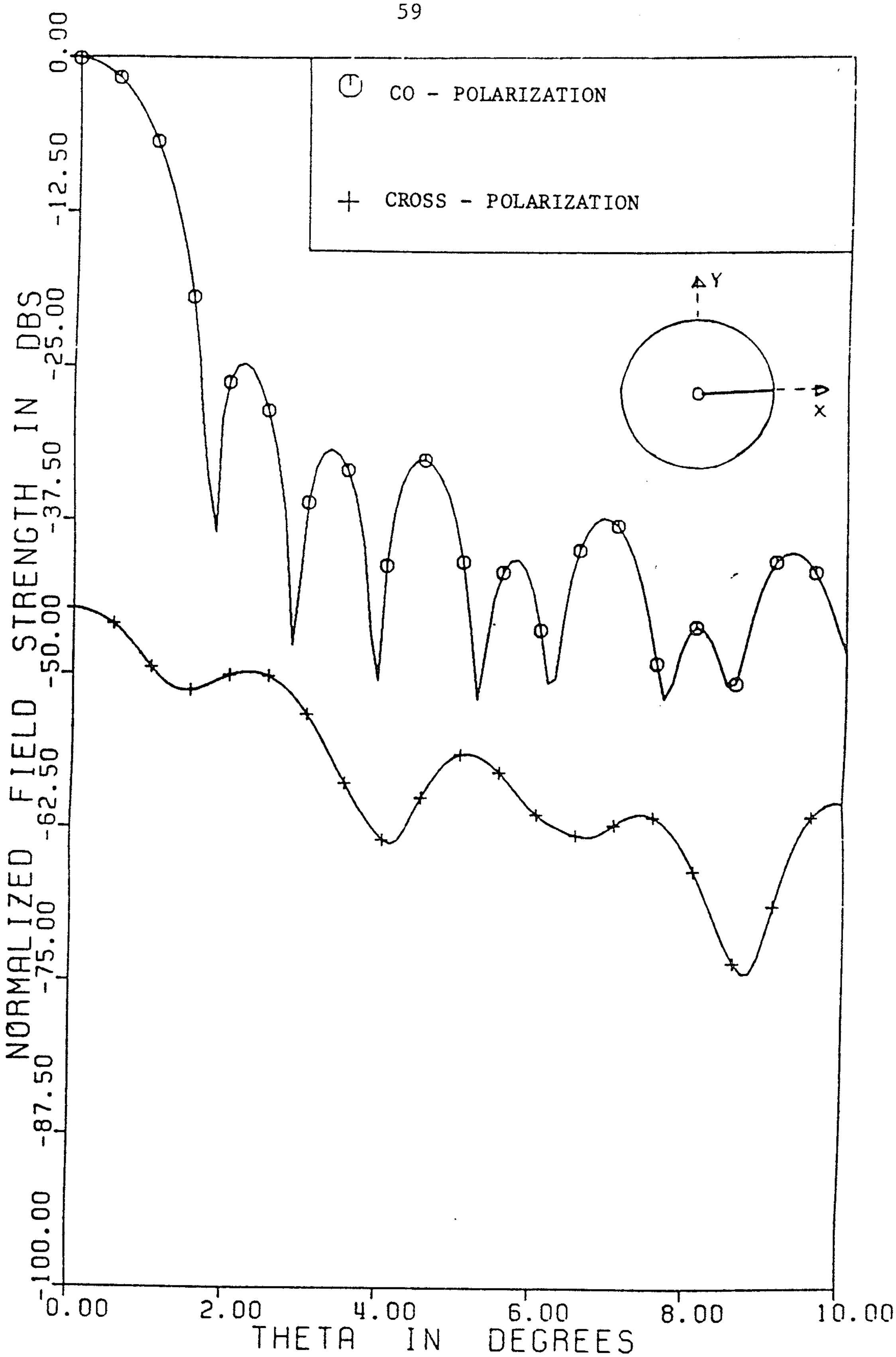

Figure 3.22. Single strut co-polar and cross - polar patterns of a circular polarization feed with a cos θ illumination , $\phi = 45^0$, a = 0.25 λ .

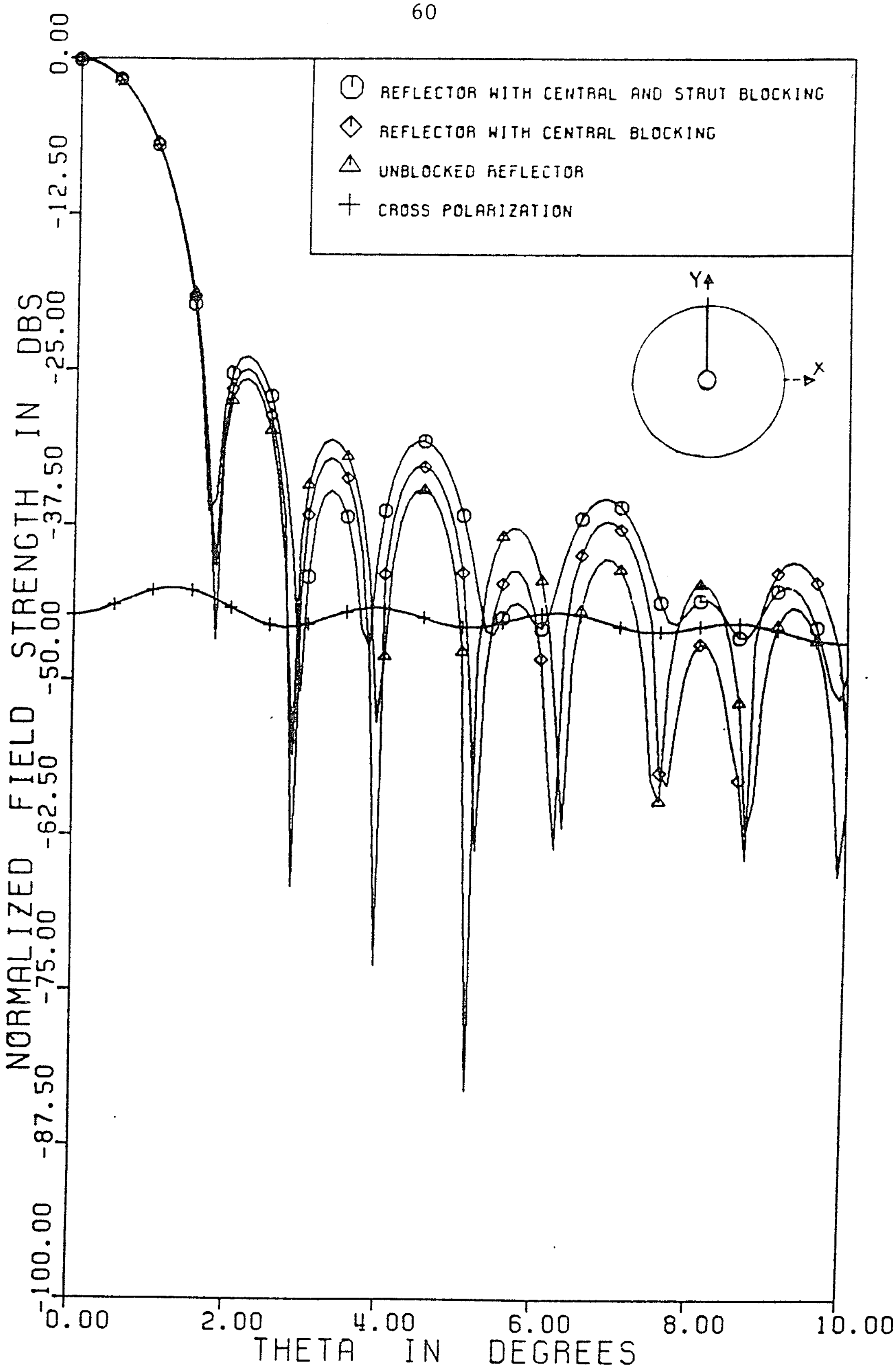

Figure 3.23. Single strut co-polar and cross - polar patterns with cos θ illumination , $\phi = 0^0$ plane , $a = 0.25\ \lambda$, circular polarization .

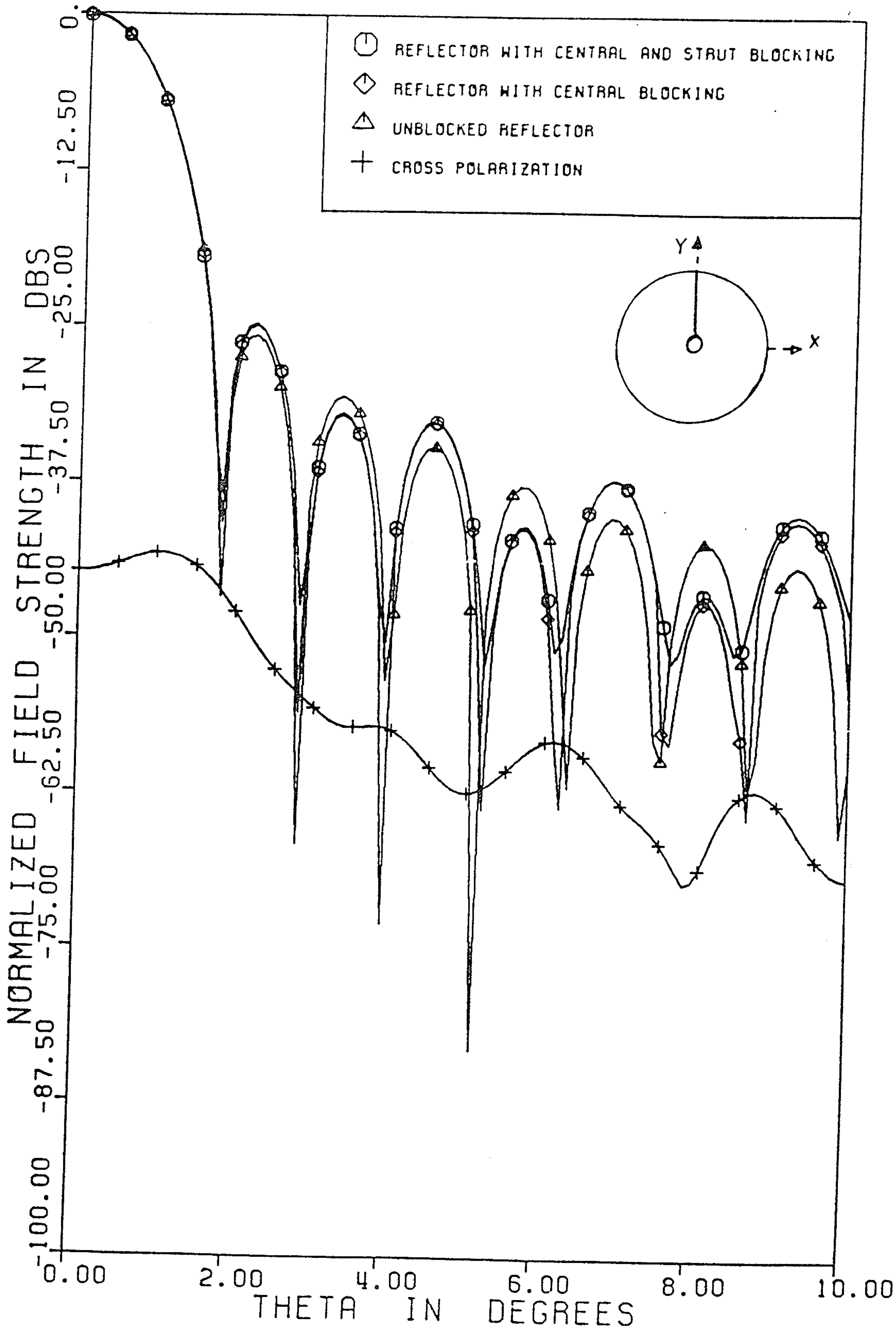

Figure 3.24. Single strut co-polar and cross - polar patterns with cos θ illumination , $\phi = 45^0$ plane , $\bar{a} = 0.25\ \lambda$, circular polarization

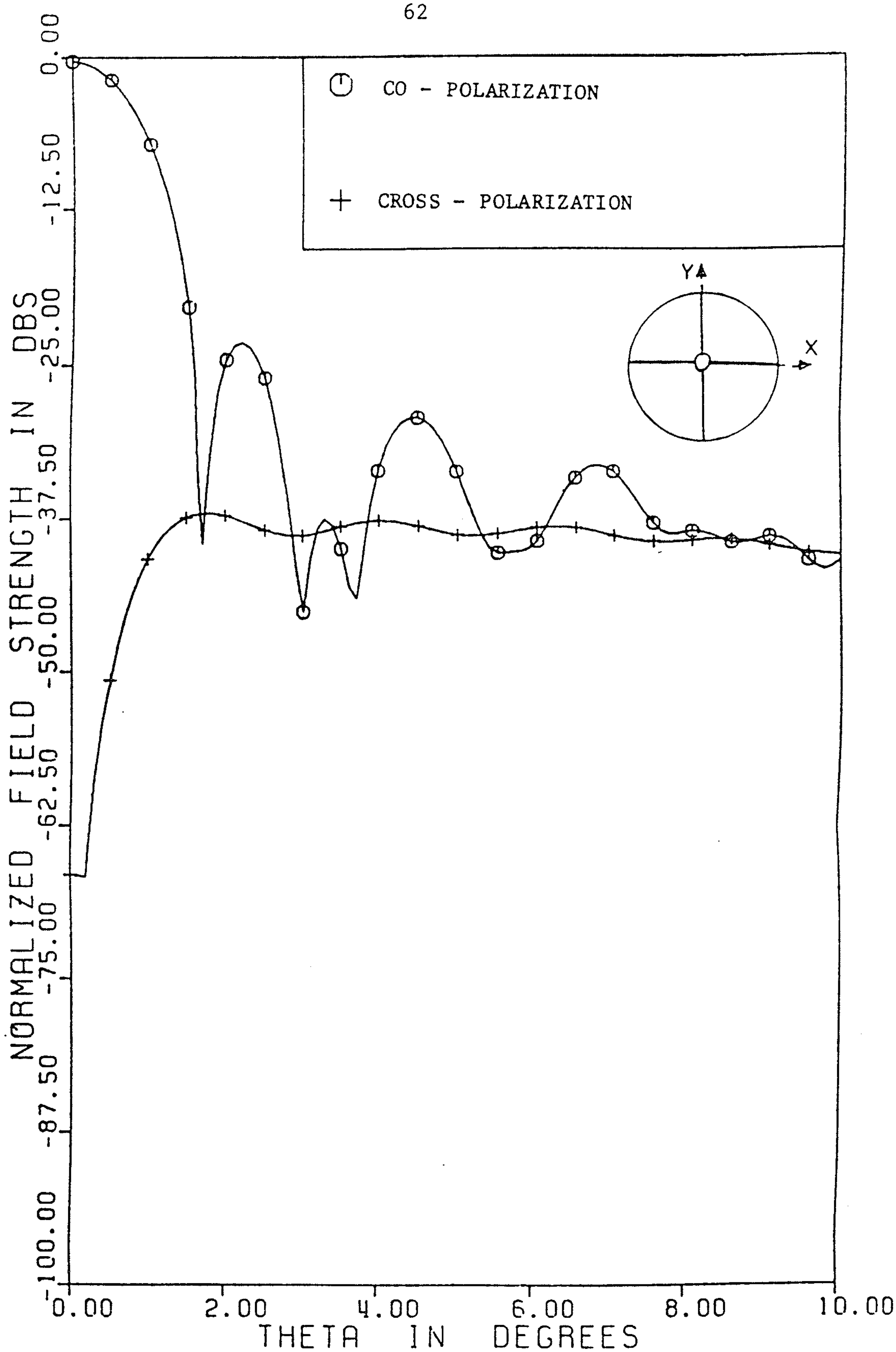

Figure 3.25. Quad co-polar and cross - polar patterns of a circular polarization feed with a cos θ illumination , $\phi = 0^0$ and 90^0 , $a = 0.25\ \lambda$.

CHAPTER IV

SIDELOBE REDUCTION

4.1 Introduction

In the last chapter, computed data for the effects of central and strut blockage on the reflector sidelobe levels were presented. It was found that for a single strut geometry the sidelobe levels are generally satisfactory as long as the strut is not located along the E-plane. The results for a tripod were also satisfactory. However, for a quad-strut geometry the situation was quite different. The overall patterns were poor and for the E-plane struts all near-in sidelobes had very high levels. In this chapter we will attempt to study possible means of reducing the sidelobe levels. The problem will be discussed briefly and a useful method will be proposed.

Many possible techniques may be used for sidelobe reduction. From the mechanical point of view it is advantageous to select another cross-section, such as square or rectangular that has better bending characteristics. For these arbitrary strut cross-sections the scattered field cannot, in general, be found analytically and a numerical method must be used. A major disadvantage of non-circular struts is their generation of high cross-polarization level. While these struts may, in certain cases, affect the co-polar sidelobes by a lesser amount, they will generate much larger cross-polar fields [5]. For this reason we have selected circular struts for the present investigation. However we could expect that by a proper selection of strut cross-sectional dimensions one may obtain improved sidelobe levels.

Non-metallic struts may also be used for sidelobe reduction. By selecting an appropriate dielectric rod diameter one may reduce the strut scattered field to levels lower than those of the conducting ones. However, dielectric rods are, generally, good scatterers for the H-polarization of the incident field. Thus, while using dielectric rods may reduce the scattered field of the E-plane struts, they will increase the scattered field of the H-plane ones. In practice, therefore, the overall scattered field of dielectric struts may not be smaller than that of conducting ones. Dielectric struts also have additional disadvantages in aging and other environmental effects. For small earth-stations a major problem lies in the focusing of sun on the struts, which in the dielectric rod case will certainly cause a complete failure of the strut.

Another technique for sidelobe reduction is the dielectric loading of struts. This approach may be used in two different ways, one to lower the scattering cross-section of the struts and the other to use the dielectric loading to cause a phase shift in the scattered field. The first approach is useful whenever the polarization of the field can be fixed with respect to the strut directions and only the E-plane struts are coated. Otherwise the reduction of the scattering by the E-plane struts may be compensated for by the increase in the scattering of the H-plane ones. In yet another method one may select dielectric dimensions to cause a proper phase relationship beetween the reflector and the strut fields. However, this method still has the same disadvantage of the last technique involving dielectric materials.

An alternative technique for sidelobe reduction is the aperture field phase shifting by loading the reflector surface by narrow strips of appropriate thicknesses, just under each strut. Practically, this technique seems applicable. In the next section, this approach is studied analytically and the geometries are modelled approximately. It is therefore expected that the computed data be approximate and their accuracy must be examined experimentally. In particular, even if the method may be found satisfactory by the experiment, the optimization of the proposed geometries must be carried out experimentally.

4.2 Aperture Field Phase Shifting

Generally, scattered field of a conductor has a phase difference with the incident field by about 180°. For this reason, the scattered fields due to the struts tend to reduce the gain of the reflector and cause the pattern deterioration. From this property of the scattered field one therefore can expect that, any method that can be used to reverse the phase of the illuminating field of the blocked area, it may remedy the sidelobe deterioration of the antenna. Here we intend to explore one possibility. We propose to use metallic strips on the reflector surface, just under each strut, so that the reflecting surface is raised by the thickness of the strip, γ. In this manner, the field illuminating the struts will travel shorter distance and consequently the field illuminating the struts will have a phase difference with the aperture field. If the thickness of the strips is selected properly this phase difference will compensate for the phase reversal due to struts and their scattered field will become in phase in the axial direction. Thus, the effect of the struts scattered field can be used beneficially to enhance the gain and to reduce the sidelobe levels, rather than to increase them.

For quad-strut geometry the configuration of the strips on the reflector is shown in Figure (4.1). To simplify the analysis we assume the current distribution on the strips to be the physical optics currents. This assumption is a crude one, since the width of the strips is small and their current distribution is not exactly close to the physical optics current. Nevertheless, it will provide a reasonable answer to the problem at hand. For a precise analysis one must use the actual current on the strips. With the assumed physical optics currents on the strip we have computed the new reflector patterns and the strut scattered field. The generated data were examined for various strip thicknesses and an optimum thickness for each strut configuration was found. It was realized that a thickness of between 0.35λ to 0.45λ generally gives a satisfactory result.

For a tripod configuration the representative patterns for a strip thickness of 0.35λ are shown in Figure (4.2), where a $\cos\theta$ feed illumination was assumed and the strut diameter was 0.5λ. It is evident that the sidelobes are reduced considerably and the pattern first sidelobe is lowered below that of the unblocked aperture. The corresponding efficiencies are shown in Table (4.1), which show an enhancement of the gain and the efficiency.

For a quad strut configuration the computed patterns for two strip thicknesses are shown in Figures (4.3) and (4.4). For a 0.35λ strip thickness, Figure (4.3) shows a useful reduction of the sidelobe below that of the unblocked aperture and an enhancement of the gain. Figure (4.4) on the other hand, indicates a reduction of the higher order sidelobes at the expense of the first sidelobe and the gain. The corresponding efficiences are also shown in Table (4.1).

The patterns of the last three cases are computed again under the same conditions but for a circularly polarized feed. The representative patterns are shown in Figures (4.5) to (4.7). It is seen that the strip loading of the reflector improves its radiation pattern for the circularly polarized feed similar to the case of a linearly polarized feed.

From these data it is clear that, loading the reflector surface with appropriately selected conductors improves the antenna gain and overcomes the problem of the aperture blockage. With a properly selected conductors one can, in fact, improve the reflector patterns over that of the unblocked reflector. However, as it was pointed out, this analysis is approximate and the optimized strip thickness may not in practice be optimum. The correct strip dimension must in practice be found experimentally. This analysis only serves the purpose of indicating that the blocked aperture patterns can be improved considerably by loading the reflector surface.

TABLE 4.1

Efficiences of a Loaded Reflector

Dimensions Same as Table 3.1, cos θ

Illumination, Strip thickness = 0.35λ or 0.45λ

Spillover power	5.69%
Unblocked efficiency η_o	82.8%
Unblocked gain G_o	42.75 dB
Blocked efficiency η_B	
(i) Tripod struts with strip thickness 0.35λ	81.13%
(ii) Quad struts with strip thickness 0.35λ	80.85%
(iii) Quad struts with strip thickness 0.45λ	76.85%
Blocked gain G_B	
(i) Tripod struts with strip thickness 0.35λ	42.66 dB
(ii) Quad struts with strip thickness 0.35λ	42.65 dB
(iii) Quad struts with strip thickness 0.45λ	42.42 dB

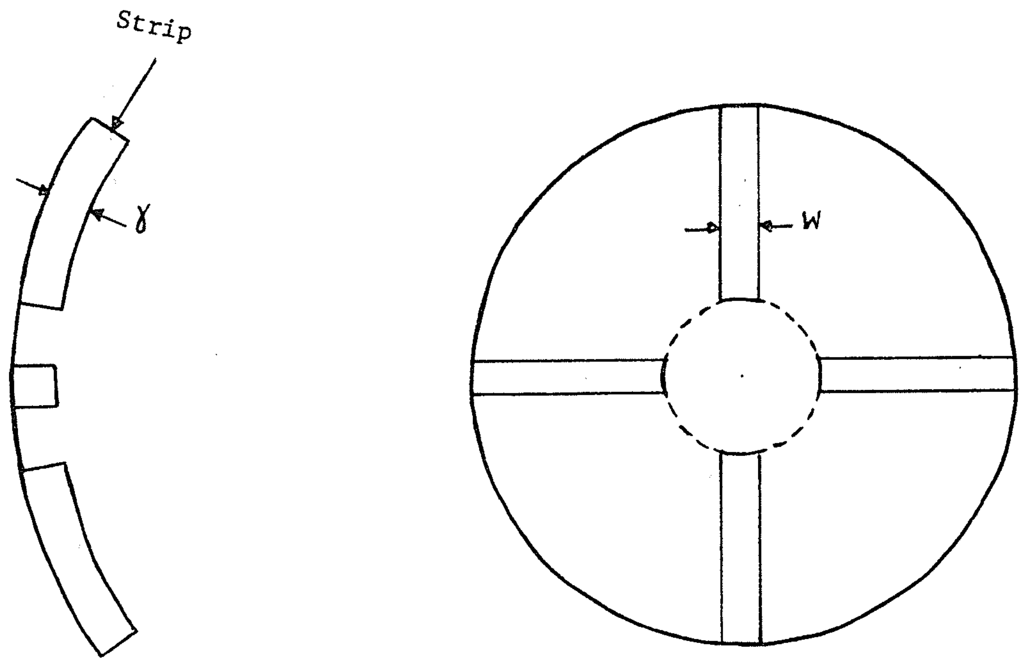

Figure 4.1. Geometry of the strip loaded reflector for a quad-strut configuration .

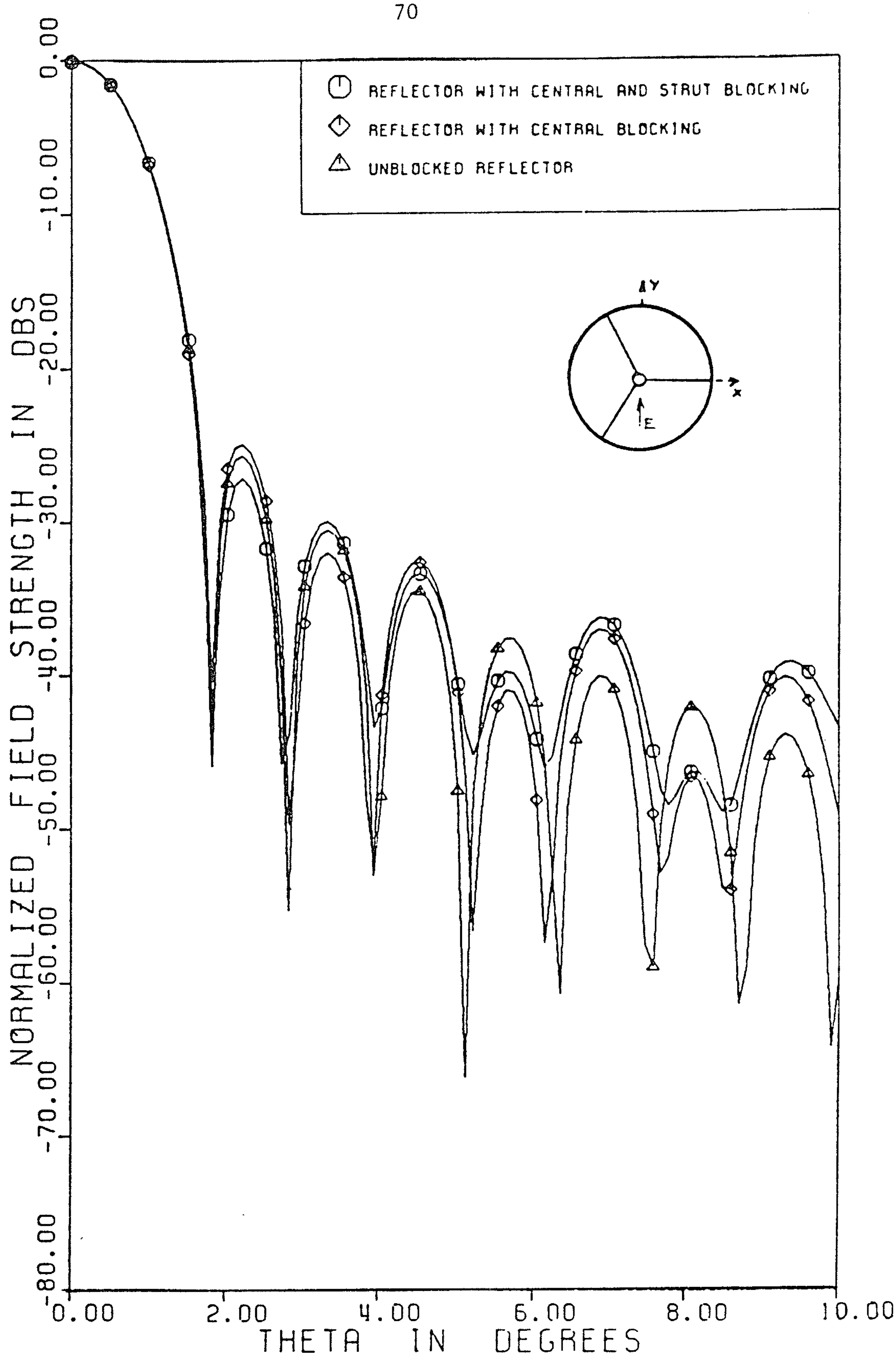

Figure 4.2. Patterns of tripod struts with strip corrected reflector, $\gamma = 0.35\ \lambda$, $\phi = 0^0$ plane, y - polarization.

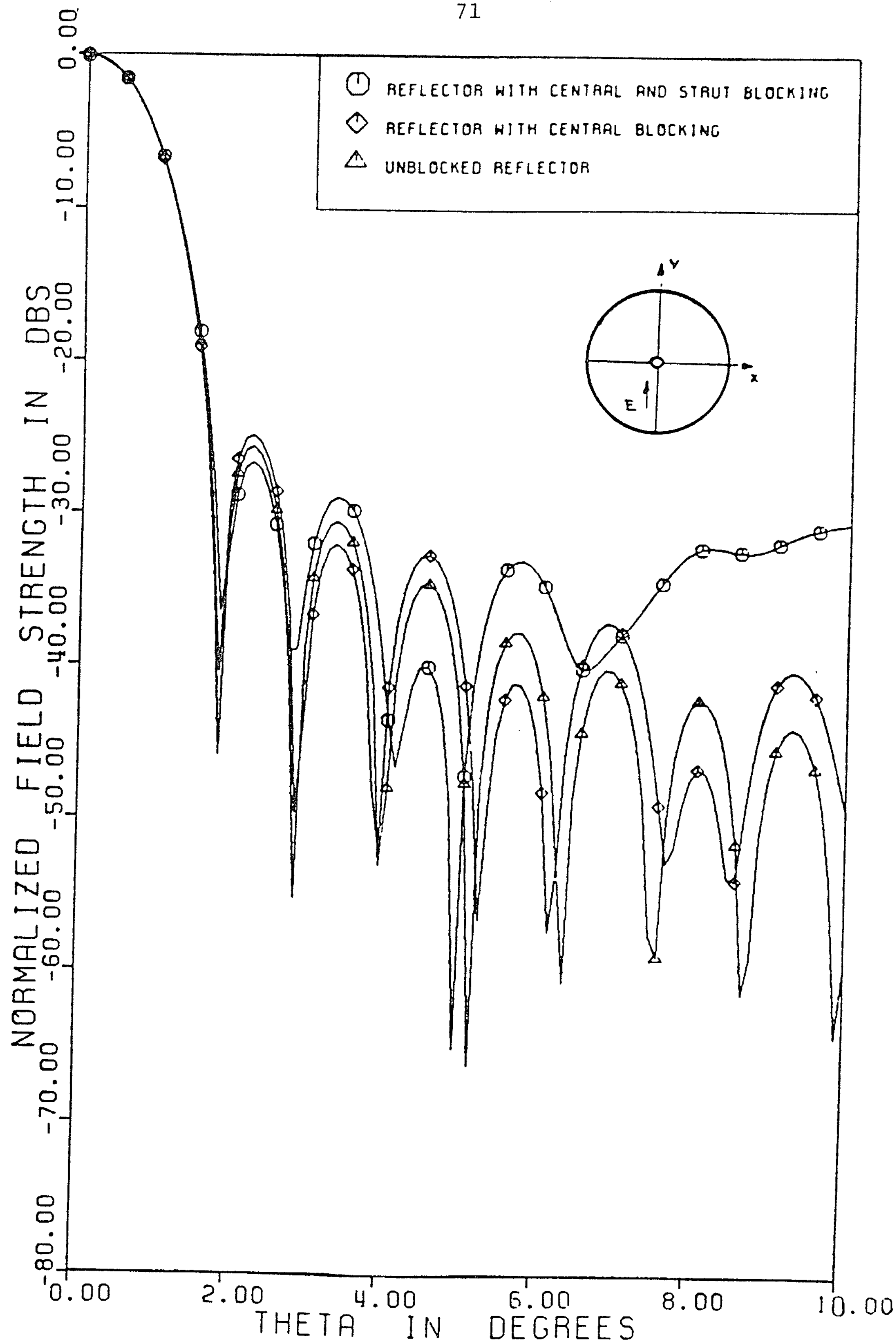

Figure 4.3. Patterns of quad struts with strip corrected reflector, $\gamma = 0.35\ \lambda$, $\phi = 0^0$ plane, y - polarization.

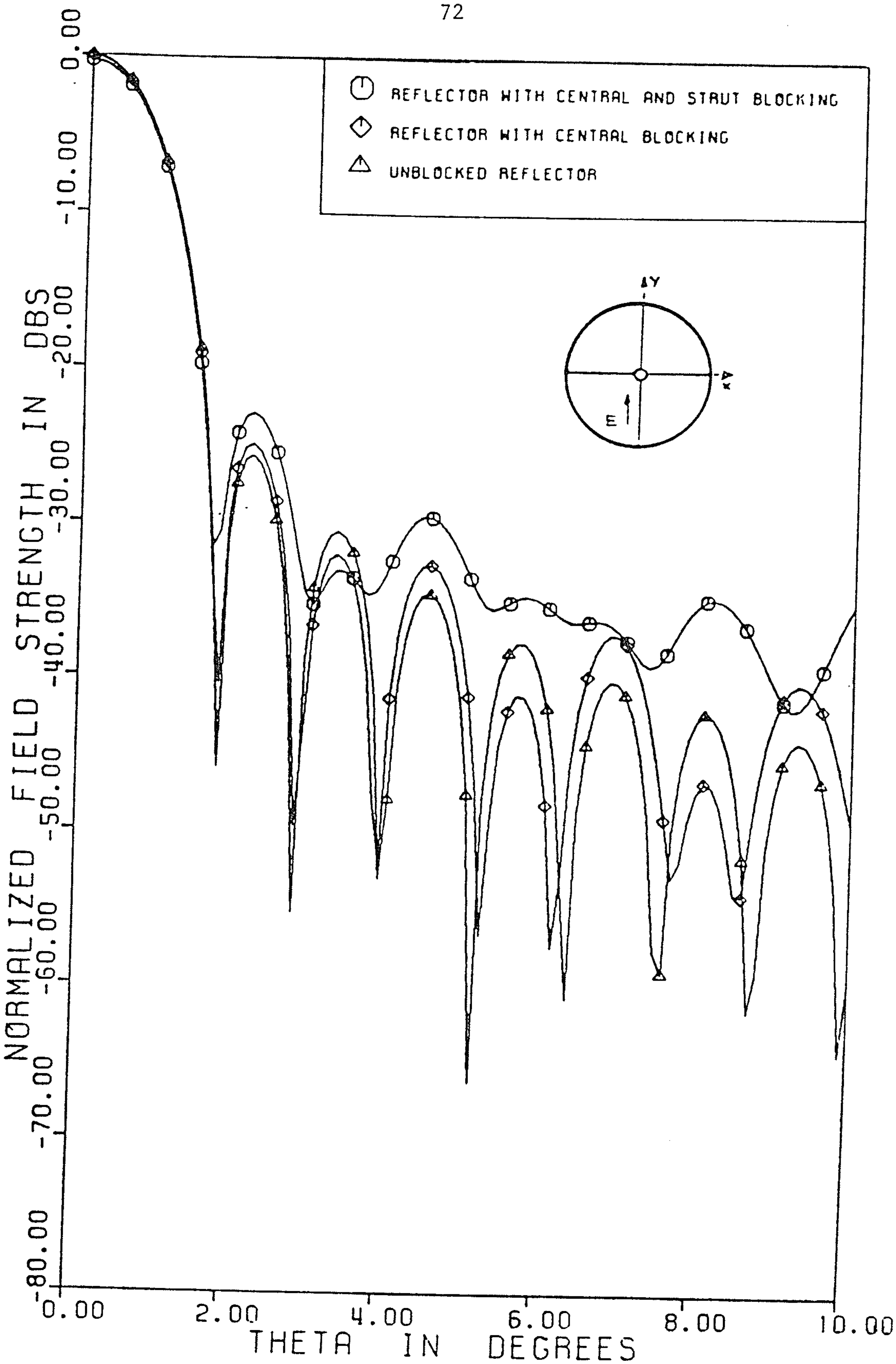

Figure 4.4. Patterns of quad struts with strip corrected reflector, $\gamma = 0.45\ \lambda$, $\phi = 0^0$ plane , y - polarization .

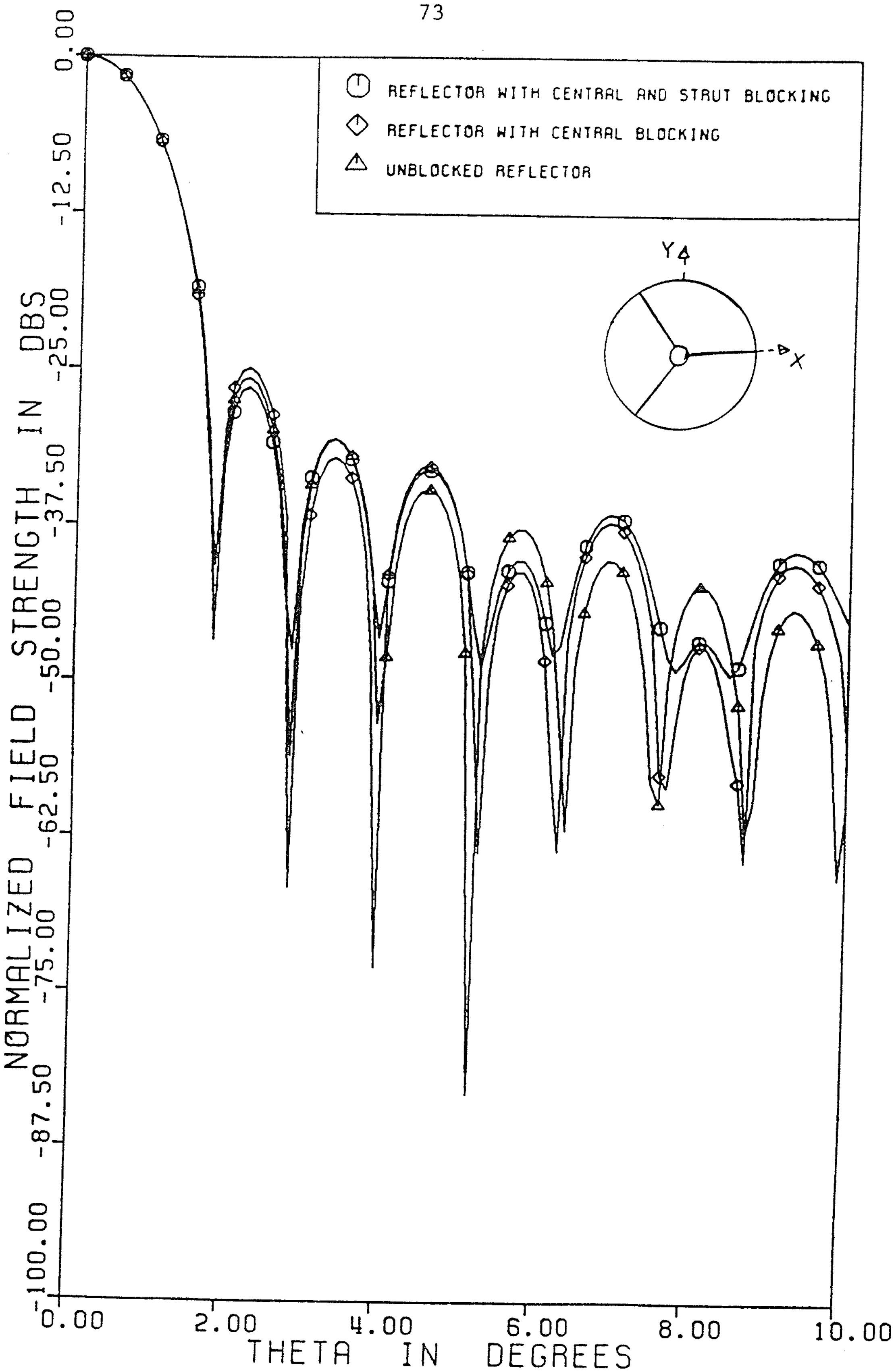

Figure 4.5. Patterns of tripod struts with strip corrected reflector, $\gamma = 0.35\ \lambda$, $\phi = 0^0$ plane, circular polarization.

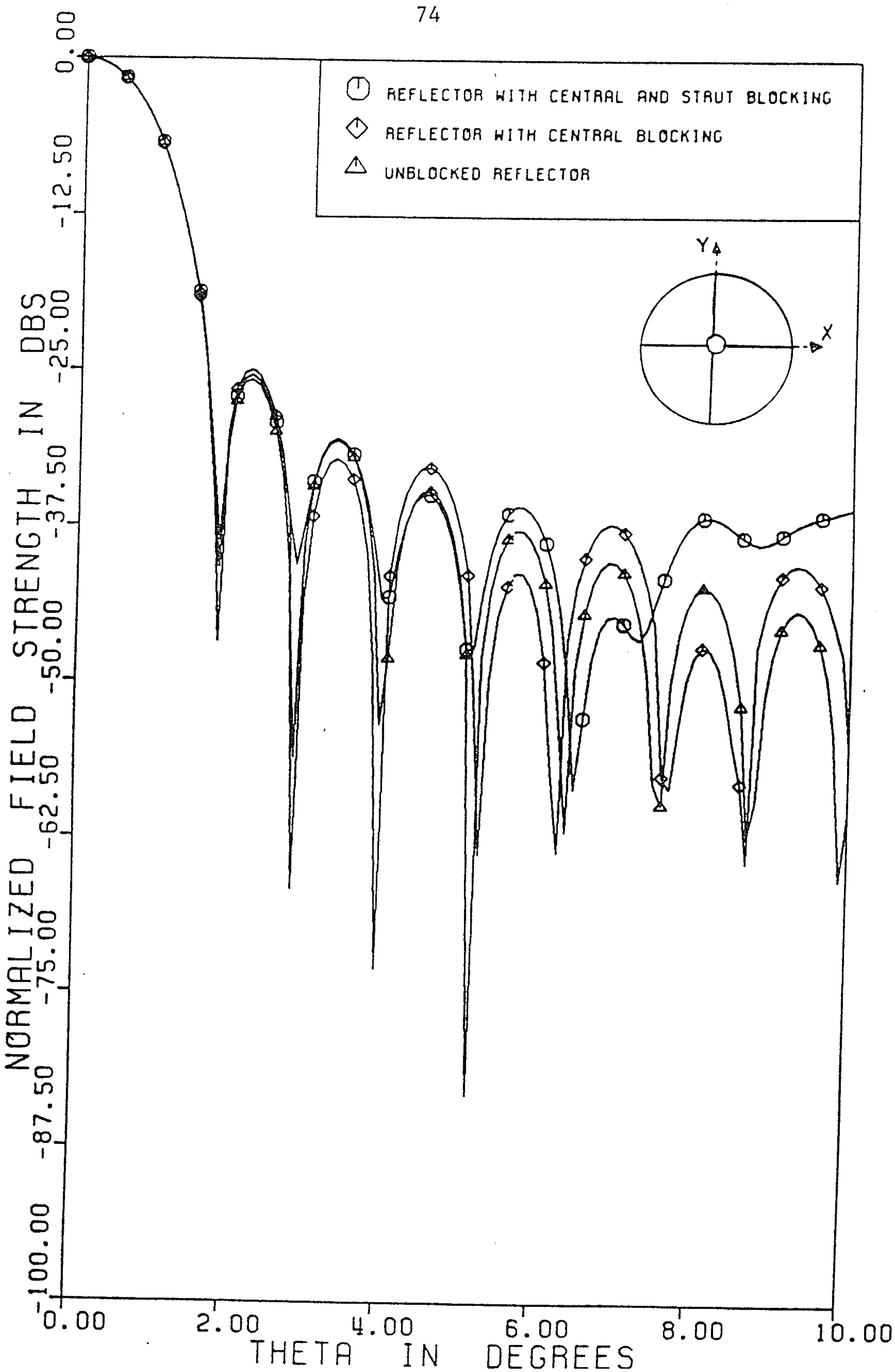

Figure 4.6. Patterns of quad struts with strip corrected reflector, $\gamma = 0.35\,\lambda$, $\phi = 0^0$ plane, circular polarization.

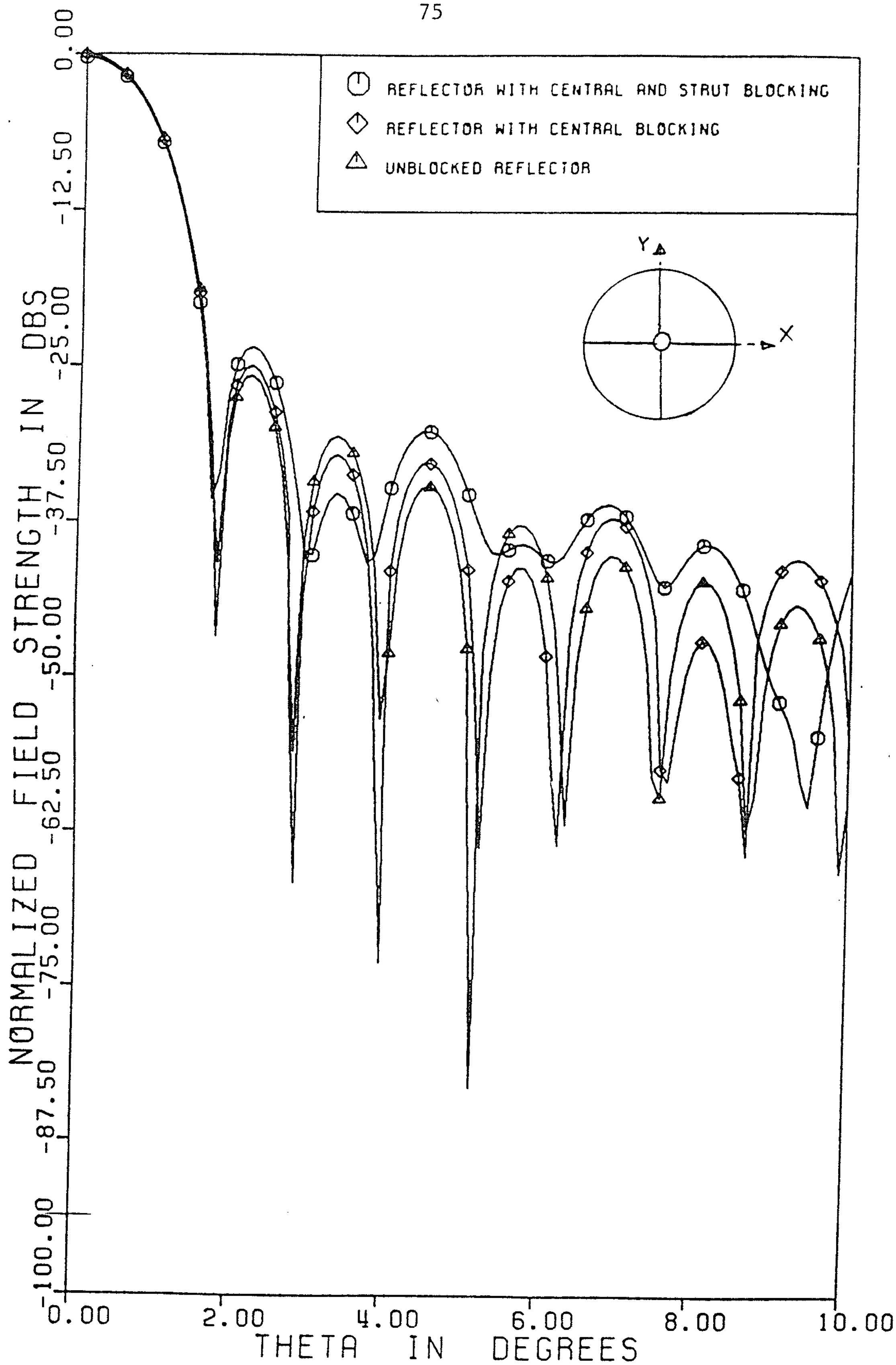

Figure 4.7. Patterns of quad struts with strip corrected reflector, $\gamma = 0.45\ \lambda$, $\phi = 0^0$ plane , circular polarization .

CHAPTER V

CONCLUSIONS AND RECOMMENDATIONS FOR FUTURE WORK

Aperture blocking of a symmetric parabolic reflector antennas has been studied. Mathematical expressions for unblocked and blocked reflector pattern calculations using current distribution method were developed and a computer program was written. The central blockage, due to the feed, has been studied using the surface current cancellation method. Struts of circular cross-section were chosen and their blocking equations obtained using the approximation of infinite struts.

Three strut configurations were considered: a single strut, a tripod configuration and a quad-strut geometry. In all cases the struts were assumed to be supported from the reflector edge, so that the full plane wave blockage of the reflector existed. In all cases, the reflector diameter was kept at 48 , with a focal length to diameter ratio of 0.375, a strut diameter of 0.5 and a central blockage diameter of 2.5 . A simplified feed model in the form of $\cos^m$ illumination was selected and the expected co-polar and cross-polar behaviours of different struct configurations were studied.

It was shown that in all cases, with a linearly polarized feed along the y-axis, the tapering of the aperture field reduced the sidelobe level, but the blockage affects the sidelobe levels of the heavily tapered illumination more significantly. The cross-polarization, in all cases, was found to be satisfactory.

For a single strut it was found that when the polarization of the feed was along the strut, the effect of the scattered field of the strut on the reflector pattern is larger. Also, provided that the struts are not along the E-plane, the blockage effect of a tripod on the sidelobes was smaller than that of a single strut along the feed polarization. On the other hand, for a quad configuration, the sidelobe levels were found to have the highest level due to the fact that two struts were selected along the E-polarization. The effect of the strut diameter on the reflector pattern was also indicated. It was shown that the diameter of the strut has a strong effect on the results.

The performance of the symmetric reflector with a circularly-polarized feed was also studied. It was found that the co-polar patterns were either similar or very near (a slightly lower sidelobe levels) to the co-polar patterns of a y-polarized feed. The cross-polarization levels were either equal to or somewhat higher than those of a y-polarized feed, except in the principal planes where the cross-polarization levels were generally very high compared with an approximately vanishing value in the case of a y-polarized feed. It was also seen that in the case of a quad-strut configuration in the 45° plane, the struts have a minimal effect on the reflector radiation pattern.

Some possible techniques for reducing the sidelobes of a symmetric reflector were discussed. It was then concluded that the most promising approach was to load the reflector with conducting strips under each strut. Because, this method was analyzed approximately, it was recommended that this method of sidelobe reduction be studied experimentally.

As a recommendation for future work, we feel that the loading of the reflector must be handled carefully. Attaching strips to the reflector may not perform satisfactorily, since strip currents between the strip and the reflector surface may destroy the predicted behaviour. Thus, either strips must be carefully shorted electrically to the reflector or other geometries such as knife edge conductors be employed. In all cases the reflector performance must be evaluated experimentally so that the optimum configuration may be obtained.

REFERENCES

[1] SILVER, S., "Microwave Antenna Theory and Design", McGraw-Hill Book Co., New York, 1949.

[2] CHUGH, R.K., "Dielectric Cone Feed Reflecting Antennas", Ph.D. Thesis, University of Manitoba, 1977.

[3] CLARRICOATS, P.J.B. and POULTON, G.T., "High-Efficiency Microwave Reflector Antennas - A Review", Proc. IEEE, Vol. 65, No. 10, pp. 1470-1504, October 1977.

[4] RUDGE, A.W. and ADATIA, N.A., "Offset-Parabolic-Reflector Antennas: A Review", Proc. IEEE,Vol. 66, No. 12, pp. 1592 - 1618, December 1978.

[5] SHAFAI, L., "To Study State-of-the Art Techniques to Improve Sidelobe Characteristics of Small Earth-Station Reflector Antennas", Final Report, DSS File No. 03SU,36001-1-3247, Contract Serial No. OSU81-00450, University of Manitoba, Winnipeg, Manitoba, May, 1982.

[6] CRAY, C.L., "Estimating the Effect of Feed Support Member Blocking on Antenna Gain and Side-lobe Level", Microwave Journal, March, 1964, pp. 88-91.

[7] RUSCH, W.V.T. and POTTER, P.D., "Analysis of Reflector Antennas", Academic Press, New York, 1970.

[8] RUSCH, W.V.T., and SORENSEN, O., "Aperture Blockage of a Focused Paraboloid", Final Report, ESTEC/Contract No. 2170/74 JS, Electromagnetic Institute, Denmark, 1974.

[9] RUSCH, W.V.T., HANSEN, J.A., KLEIN, C.A., and MITTRA, R., "Forward Scattering from Square Cylinders in the Resonance Region with Application to Aperture Blockage", IEEE Trans. on Antennas and Propogation, AP-24, No. 2, pp. 182-189, March 1976.

[10] KAY, A.F., "Electrical Design of Metal Space Frame Radoms", IEEE Trans on Antennas and Propogation, AP-13, No. 2, pp. 188-202, March 1965.

[11] RUZE, J., "Feed Support Blockage Loss in Parabolic Antennas", Microwave Journal, Vol. 11, No. 12, 1968, pp. 76-80.

[12] KUEHL, H.H., "Radiation From a Radial Electric Dipole Near a Long, Finite Circular Cylinder", IRE trans. on Antennas and Propagation, AP-9, No. 6, Nov. 1961, pp. 546-553.

[13] JAMES, G.L. and KERDEMLIDIS, "Reflector Antenna Radiation Pattern Analysis by Equivalent Edge Currents", IEEE Trans. on Antennas and Propagation, AP-21, pp. 19-24, January 1973.

[14] RUSCH, W.V.T. and SORENSEN, O., "The Geometrical Theory of Diffraction for Axially Symmetric Reflectors", IEEE Trans on Antennas and Propogation, AP-23, pp. 414-419, May 1975.

[15] TSAI, L.L., WILTON, D.R., HARRISON. M.G. and WRIGHT, E.H., "A Comparison of Geometrical Theory of Diffraction and Integral Equation Formulation for Analysis of Reflector Antennas", IEEE Trans. on Antennas and Propagation, AP-20, pp. 705-712, November 1972.

[16] CLARRICOATS, P.J.B., "Some Recent Advances In Microwave Reflector Antennas", Proc. IEE, Vol. 126, No. 1, pp. 9-25, January 1979.

[17] LUDWIG, A.C., "The Definition of Cross Polarization", IEEE Trans. on Antennas and Propagation, AP-21, pp. 116-119, January 1973.

[18] GHOBRIAL, S.I., "Co-Polar and Cross-Polar Diffraction Images in the Focal Plane of Paraboloidal Reflectors: A Comparison Between Linear and Circular Polarization", IEEE Trans. on Antennas and Propagation, AP-24, No. 4, pp. 418-424, July 1976.

[19] ABRAMOWITZ, M. and STEGUN, I.A. "Handbook of Mathematical Functions", Dover Publications, New York, 1965.

[20] COLLIN, R.E. and ZUCKER, F.J., "Antenna Theory" Pt. 1 and Pt. 2, McGraw-Hill Book Co., New York, 1969.

[21] HARRINGTON, R.F., "Time-Harmonic Electromagnetic Fields", McGraw-Hill Book Co., New York, 1961.

[22] KRAUS, J.D., "Antennas", McGraw-Hill Co., New York, 1950.